nature communications

Article

https://doi.org/10.1038/s41467-025-62417-2

Fbxo42 promotes the degradation of Ataxin-2 granules to trigger terminal Xbp1 signaling

Received: 8 November 2024

Accepted: 16 July 2025

Published online: 13 August 2025

Check for updates

Cristiana C. Santos[1], Nadine Schweizer[1], Fátima Cairrão[1], Juanma Ramirez[2], Nerea Osinalde[2], Ming Yang[3], Catarina J. Gaspar[1,7], Vanya I. Rasheva[1], Miguel L. Trigo[1], Zach Hensel[1], Colin Adrain[4], Tiago N. Cordeiro[1], Franka Voigt[3], Paulo A. Gameiro[5], Ugo Mayor[2,6] & Pedro M. Domingos[1]

The Unfolded Protein Response (UPR) is activated by the accumulation of misfolded proteins in the Endoplasmic Reticulum (ER), a condition known as ER stress. Prolonged ER stress and UPR activation cause cell death, by mechanisms that remain poorly understood. Here, we report that regulation of Ataxin-2 by Fbxo42 is a crucial step during UPR-induced cell death. From a genetic screen in *Drosophila*, we identify loss of function mutations in *Fbxo42* that suppress cell death and retinal degeneration induced by the over-expression of Xbp1^{spliced}, an important mediator of the UPR. We identify the RNA binding protein Ataxin-2 as a substrate of Fbxo42, which, as part of a Skp-A/Cullin-1 complex, promotes the ubiquitylation and degradation of Ataxin-2. Upon ER-stress, the mRNA of Xbp1 is sequestered and stabilized in Ataxin-2 granules, where it remains untranslated. Fbxo42 recruitment to these granules promotes the degradation of Ataxin-2, allowing for the translation of Xbp1 mRNA and triggering cell death during the terminal stages of UPR activation.

The Endoplasmic Reticulum (ER) is the cell organelle where secretory and membrane proteins are synthesized and folded. When the folding capacity of the ER is impaired, the presence of unfolded or incorrectly folded (misfolded) proteins in the ER causes stress on the cell - ER stress - and activates the Unfolded Protein Response (UPR), to restore homeostasis in the ER[1].

The UPR is accomplished via the activation of signaling pathways induced by 3 ER transmembrane molecular sensors that detect ER stress: Inositol-requiring enzyme 1 (Ire1), Pancreatic ER kinase (PKR)-like ER kinase (Perk) and Activating transcription factor 6 (Atf6). The activation of the UPR leads to the reduction of general protein synthesis, to prevent further accumulation of proteins in the ER, and the transcriptional up-regulation of a specific subset of genes, including genes encoding ER chaperones and enzymes, to increase the protein folding capacity of the ER. However, when ER stress is prolonged and severe, leading to chronic activation of the UPR, cells can activate apoptosis, a genetic programmed form of cell death, by mechanisms that are still poorly understood[2,3].

The transcription factor Xbp1 is an important mediator of Ire1 signaling. Upon the activation of the UPR, the endoribonuclease domain of Ire1 cleaves the Xbp1 mRNA in two sites, a non-conventional splicing event that causes a frameshift during translation, introducing a longer carboxyl domain in the protein encoded by Xbp1^{spliced} (Xbp1s) mRNA[1]. Only Xbp1^{spliced} is fully active as a transcription factor that regulates the expression of ER chaperones and other target genes[4].

Here, we find that persistent expression of Xbp1^{spliced} (Xbp1s) induces cell death, generating a smaller, atrophic “glossy” eye phenotype that is suppressed by co-expression of anti-apoptotic proteins. Through genetic screening, we identified loss-of-function mutations in the F-box protein Fbxo42 that suppress cell death induced by

[1]Instituto de Tecnologia Química e Biológica António Xavier, Universidade Nova de Lisboa, Oeiras, Portugal. [2]Department of Biochemistry and Molecular Biology, University of the Basque Country (UPV/EHU), Leioa, Bizkaia, Spain. [3]Department of Molecular Life Sciences, University of Zurich, Zurich, Switzerland. [4]Patrick G Johnston Centre for Cancer Research, Queen’s University, Belfast, UK. [5]NOVA Medical School Faculdade de Ciências Médicas, NMS FCM, Universidade Nova de Lisboa, Lisboa, Portugal. [6]Ikerbasque, Basque Foundation for Science, Bilbao, Spain. [7]Present address: Department of Research Oncology, Genentech, Inc. 1 DNA Way, South San Francisco, CA, USA. e-mail: domingp@itqb.unl.pt

https://doi.org/10.1038/s41467-025-62417-2

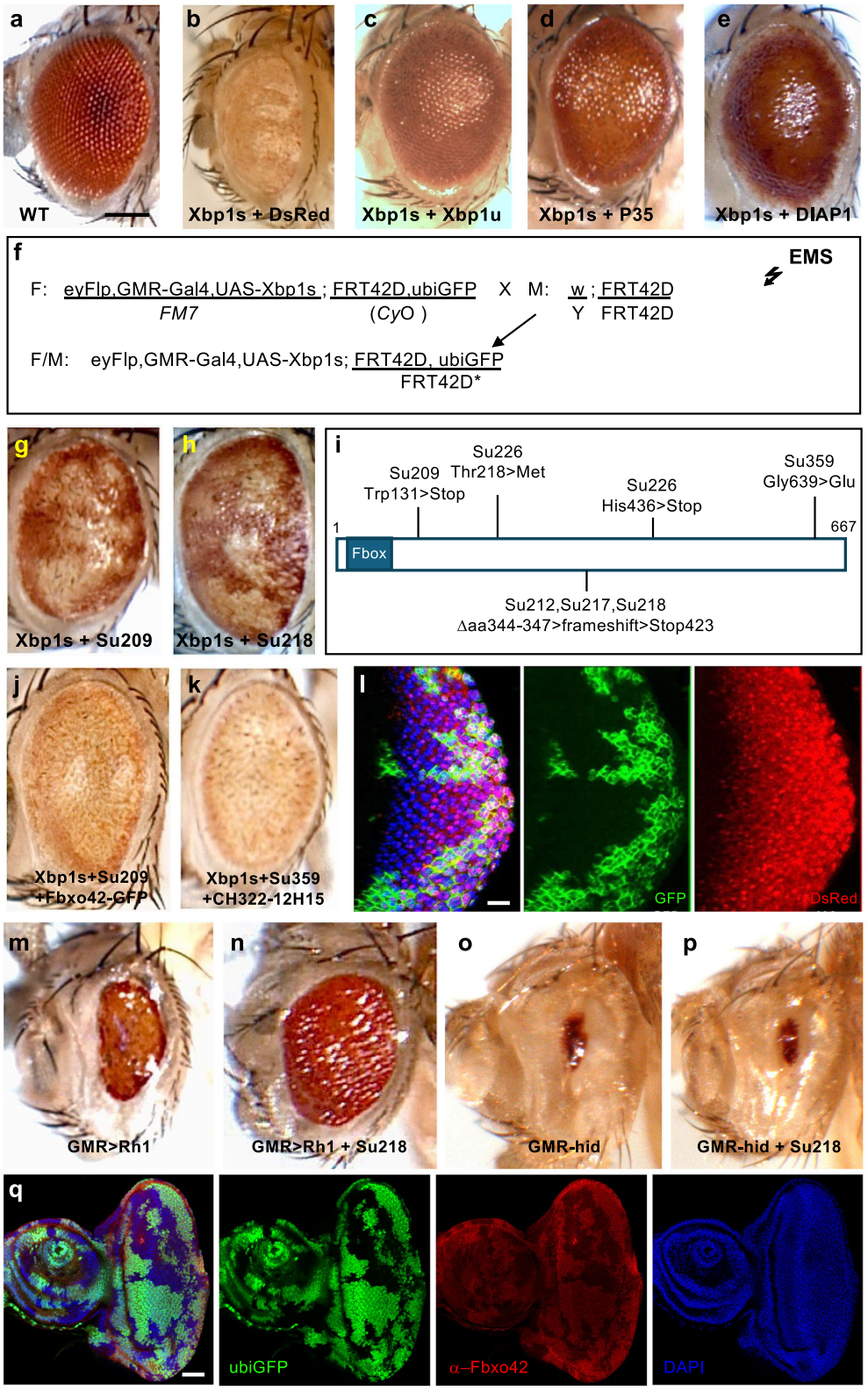

Xbp1^{spliced}. Next, we performed a proteomic screen using pulldowns with a biotinylable form of ubiquitin (^{bio}Ub) to identify the relevant substrates of Fbxo42 and discovered the RNA-binding protein Ataxin-2, as a key target. In cells undergoing high levels of ER stress, Xbp1 mRNA is initially stored in cytoplasmic Ataxin-2 granules, preventing its translation, until Fbxo42 is recruited to promote the degradation of Ataxin-2 granules, allowing for the translation of Xbp1 mRNA at terminal stages of UPR activation.

Results

Expression of Xbp1^{spliced} causes an atrophic "glossy" eye phenotype

In *Drosophila*, loss-of-function mutations in Xbp1 increase photoreceptor degeneration caused by *ninaE* (rhodopsin-1) misfolding mutations[5]. Surprisingly, in comparison with a "wild type" *Drosophila* adult eye (Fig. 1a), expression of Xbp1^{spliced} under the control of GMR-GAL4 causes a smaller, atrophic "glossy" eye phenotype (Fig. 1b),

Fig. 1 | Loss-of-function mutations in Fbxo42 suppress glossy eye phenotype caused by overexpression of Xbp1^{spliced}. **a** Wild-type adult *Drosophila* eye (Canton S). Posterior is to the right and dorsal to the top in this and all subsequent panels. Scale bar = 200 µm. **b** Glossy eye phenotype caused by overexpression of Xbp1^{spliced} (Xbp1s). Genotype: GMR-GAL4, UAS-Xbp1s, UAS-DsRed. **c** Glossy eye phenotype is suppressed by co-expression of Xbp1^{unspliced} (Xbp1u). Genotype: GMR-GAL4, UAS-Xbp1s, UAS-Xbp1u. **d** Glossy eye phenotype is suppressed by co-expression of caspase inhibitor P35. Genotype: GMR-GAL4, UAS-Xbp1s, UAS-P35. **e** Glossy eye phenotype is suppressed by co-expression of DIAP1. Genotype: GMR-GAL4, UAS-Xbp1s, UAS-DIAP1. **f** Genetic scheme of the FLP/FRT F1 genetic screen for suppressors of the glossy eye phenotype caused by overexpression of Xbp1s. **g** Glossy eye phenotype is suppressed by clones of suppressor 209. Genotype: eyFlp,GMR-GAL4,UAS-Xbp1s; FRT42D, Su209/FRT42D, ubiGFP. **h** Glossy eye phenotype is suppressed by clones of suppressor 218. Genotype: eyFlp,GMR-GAL4,UAS-Xbp1s; FRT42D, Su218/FRT42D, ubiGFP. **i** Schematic representation of Fbxo42 (amino acids 1–667), with the F-box domain (blue box) and the mutations found in six of the suppressor alleles (Su209, Su212, Su217, Su218, Su226 and Su359) obtained from the genetic screen. Su212, Su217 and Su218 have a small deletion that causes a frameshift and premature Stop codon at 423. **j** Overexpression of Fbxo42-GFP abolishes suppression of glossy eye by Su209. Genotype: eyFLP,GMR-GAL4,UAS-Xbp1s; FRT42D, Su209/FRT42D, ubiGFP; UAS-Fbxo42-GFP. **k** A genomic rescue construct containing Fbxo42 (Pacman CH322-12H15) abolishes suppression of glossy eye by Su359. Genotype: eyFLP,GMR-GAL4,UAS-Xbp1s; FRT42D, Su359/FRT42D, ubiGFP; CH322-12H15. **l** Immunofluorescence of 3rd instar larva eye discs containing clones of Su218, labeled by the absence of ubiGFP (green). GMR-GAL4 driven expression of UAS-DsRed is similar in Su218 and ubiGFP clones. Genotype: eyFlp,GMR-GAL4, UAS-DsRed; FRT42D, Su218/FRT42D, ubiGFP. Three independent replicates were conducted. Scale bar = 30 µm. **m** Glossy eye phenotype caused by overexpression of Rh1. Genotype: eyFlp,GMR-GAL4; FRT42D/FRT42D, GMR-hid, CL;UAS-Rh1. **n** Whole eye mutant clones of Su218 suppress glossy eye phenotype caused by overexpression of Rh1. Genotype: eyFlp,GMR-GAL4; FRT42D, Su218/FRT42D, GMR-hid, CL;UAS-Rh1**.** **o** Small eye phenotype caused by overexpression of hid. Genotype: eyFlp,GMR-hid; FRT42D/FRT42D,ubiGFP. **p** Clones of Su218 do not suppress the small eye phenotype caused by overexpression of hid. Genotype: eyFlp,GMR-hid; FRT42D, Su218/FRT42D,ubiGFP. **q** Immunofluorescence of 3rd instar larva eye discs containing clones of Su218, labeled by the absence of ubiGFP (green), with an antibody made against Fbxo42 (Red). DAPI is in blue. Genotype: eyFlp,GMR-GAL4; FRT42D, Su218/FRT42D, ubiGFP. Scale bar = 60 µm. Three independent replicates were conducted.

where the adult *Drosophila* eye becomes a thin layer of yellow cuticle due to the lack of photoreceptors, cone and the red pigment cells[6]. This "glossy" eye phenotype is suppressed by co-expression of Xbp1^{unspliced} (Xbp1u, Fig. 1c), P35 (Fig. 1d) or DIAP1 (Fig. 1e), with the partial recovery of the red pigment and the external lens structure. Partial suppression by Xbp1^{unspliced} is consistent with the role of mammalian Xbp1^{unspliced} in promoting the down-regulation of Xbp1^{spliced} signaling[7]. Partial suppression by baculovirus P35 or *Drosophila* inhibitor of apoptosis 1 (DIAP1), two anti-apoptotic proteins, indicates that apoptotic cell death plays a role in the induction of the "glossy" eye phenotype by Xbp1^{spliced}.

Mosaic expression of a control UAS-DsRed (Supplementary Fig. 1a), by the use of the Flipase/FRT technique[8], results in an adult eye where around two thirds of the cells have DsRed expression. Mosaic expression using a FRT chromosome containing both UAS-Xbp1^{spliced} and UAS-DsRed transgenes (Supplementary Fig. 1b), results in a much reduced number of DsRed positive cells that present the "glossy" phenotype. These results indicate that Xbp1^{spliced} induces the "glossy" phenotype in a cell autonomous manner and that most of the cells expressing Xbp1^{spliced} die during eye development. In fact, higher levels of apoptotic TUNEL staining are observed in 3rd instar larva eye discs containing clones of overexpression of Xbp1^{spliced}, labelled by DsRed (Supplementary Fig. 1c). We have also observed upregulation of the autophagy marker LC3-GFP by mosaic overexpression of Xbp1^{spliced} in the larval eye disc (Supplementary Fig. 1d), consistent with the results previously reported for overexpression of Xbp1^{spliced} in the fat body[9].

Loss-of-function mutations in Fbxo42 suppress Xbp1^{spliced}-induced "glossy" eye phenotype

In order to investigate the downstream molecular mechanisms involved in the induction of the "glossy" eye phenotype by Xbp1^{spliced}, we performed a F1 genetic screen where mosaic eyes were generated by the Flipase/FRT technique[8] with Ethyl methanesulfonate (EMS) mutagenized chromosomes (Fig. 1f), in the background of Xbp1^{spliced} overexpression. Around 80.000 EMS mutagenized flies were screened, leading to the identification of 33 mutations in the right arm of the second chromosome (2R) that suppress the Xbp1^{spliced} "glossy" eye phenotype.

All the mutations were crossed to each other to create complementation groups by lethality. The biggest complementation group contained 14 mutant alleles, including suppressor (Su) 209 (Fig. 1g) and Su218 (Fig. 1h, Supplementary Fig. 1e), which show clones with suppression of the "glossy" eye phenotype, with partial recovery of the red pigment and the external lens morphology in the eye. This complementation group was mapped by crossing the mutant alleles with a set of deficiencies (genomic deletions) covering 2R. From these crosses, we failed to obtain viable non-balanced progeny (except a few adult escapers with out-held wing phenotype) from Df(2R)BSC597, but we obtained viable non-balanced progeny from Df(2R)Exel7170 and Df(2R)01D01W-L133, mapping this complementation group to an interval containing 12 genes, between 58C1 and 58D1 (Supplementary Fig. 1f). Viable non-balanced progeny was obtained from crosses to Df(2R)a(7) but not from Df(2R)a(EX1). Since the distal end of Df(2 R)a(EX1) is not molecularly defined[10], we tested how far distally this deficiency reaches by crossing Df(2 R)a(EX1) to lethal P element insertions in *Vps35* (P(EP)Vps35^{EY16641} and P(EP)Vps35^{EY14200}) and *CG3074* (P(GawB)CG3074^{NP7371}). Since viable non-balanced progeny was obtained from these crosses, we concluded that Df(2R)a(EX1) does not reach *Vps35*. Also, our suppressor mutations were not lethal over the lethal P element insertions in *Vps35*. With this approach, we rendered our region of interest to six genes (*Fbxo42*, *CG3045*, *CG11170*, *CG30279*, *CG11275* and *MED16*). Since no lethal alleles existed for these genes, we sequenced genomic DNA extracted from homozygous larvae for Su218, Su359 and the isogenized FRT42D line that was subjected to EMS mutagenesis. Our first attempt was with the gene *MED16*, in which no mutations were found, but in our second attempt we found several mutations in *Fbxo42* (*CG6758*). In total, we sequenced six suppressor alleles and all had mutations in *Fbxo42*, mostly premature STOP codons (Fig. 1i).

Mosaic suppression of the "glossy" eye phenotype by Fbxo42 mutants could be rescued by overexpression of Fbxo42-GFP (Fig. 1j) or by using a Pacman genomic rescue construct (CH322-12H15) containing Fbxo42 (Fig. 1k), demonstrating that the phenotype is Fbxo42 specific. We tested UAS-DsRed expression levels in clones of Fbxo42 mutants (Su218 - Fbxo42^{N423*}) but saw no difference between the homozygous mutant and control tissue (Fig. 1l), which indicates that Fbxo42 is not required for transcriptional activation by GAL4/UAS. Su218 suppressed the strong rough eye phenotype induced by overexpression of rhodopsin-1 (Rh1) under the control of GMR-GAL4 (Fig. 1m, n), a paradigm where misfolded Rh1 accumulates in the ER, causing ER stress, activation of the UPR and Ire1-mediated splicing of Xbp1[11,12]. However, Su218 did not suppress the small eye phenotype induced by overexpression of the proapoptotic gene *hid* (Fig. 1o,p), indicating that Fbxo42 acts downstream of UPR activation but upstream of the apoptotic machinery.

The genome of *Drosophila* has 45 F-box proteins[13] that form complexes with SkpA, Cullin-1, Roc1/Rbx1 and E2 ubiquitin ligases to mediate the ubiquitylation of specific substrates. In such complexes, F-box proteins bind to SkpA through the conserved F-box domain, which is present N-terminally in Fbxo42 (Fig. 1i). In *Drosophila* S2 cells

https://doi.org/10.1038/s41467-025-62417-2

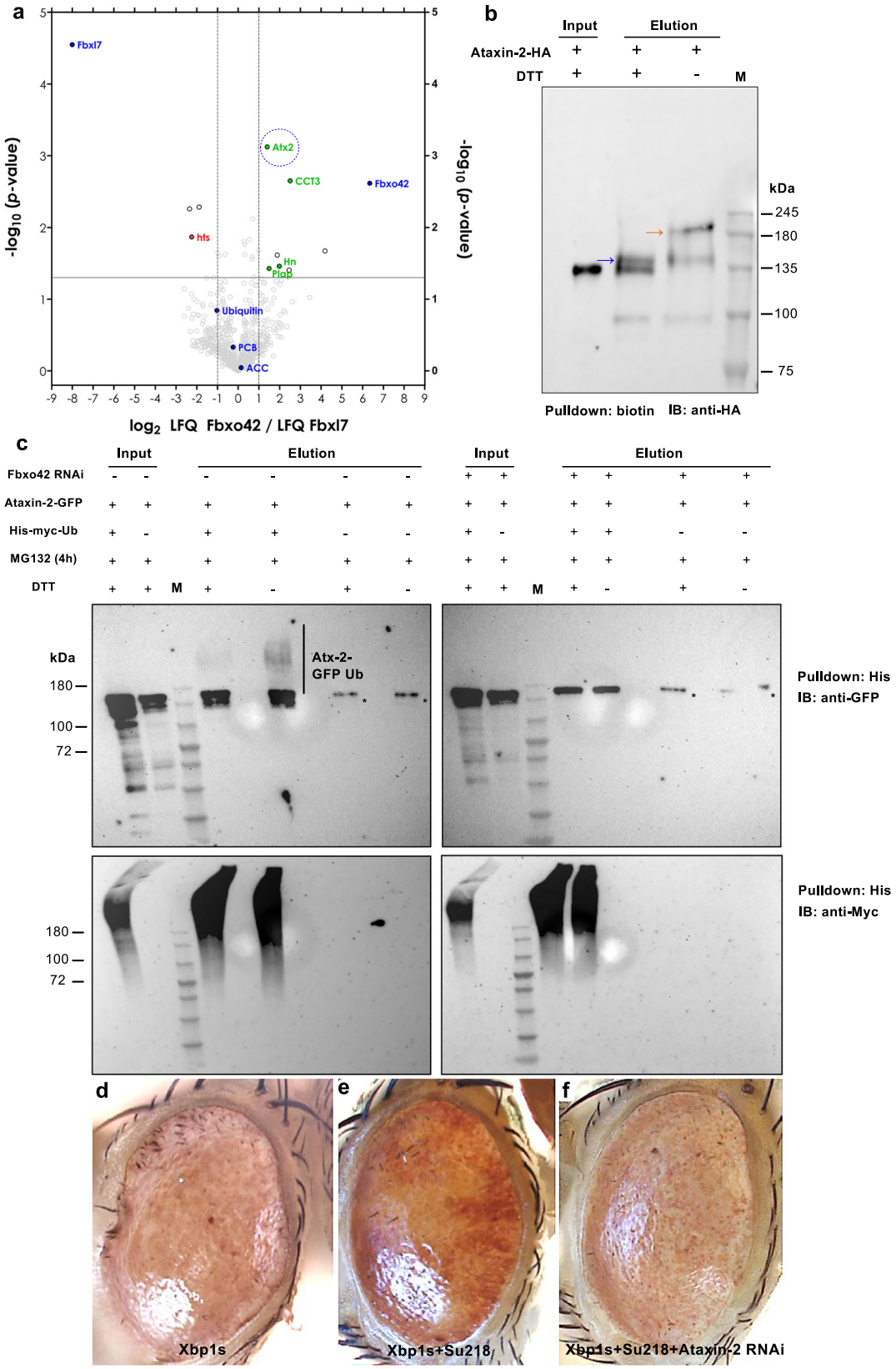

(Supplementary Fig. 1g), SkpA co-immunoprecipitates with FLAG-HA-Fbxo42, but not with a deletion of the F-box domain (FLAG-HA-ΔFbxo42), in accordance with results showing binding of Fbxo42 with SkpA in the *Drosophila* ovary[14].

We generated a rabbit polyclonal antibody raised against amino acids 384–667 of Fbxo42, which was used in immunofluorescence experiments with 3rd instar larval eye discs containing clones of Su218 ($Fbxo42^{N423*}$). Cells homozygous for Su218, labelled by the absence of ubiGFP, present reduced immunoreactivity for anti-Fbxo42, in comparison with neighboring control heterozygous cells (Fig. 1q). In immunoblots, anti-Fbxo42 detects a band just above the 72 kDa marker that is absent in larva homozygous for Su226 ($Fbxo42^{H436*}$,

Fig. 2 | Fbxo42 promotes Ataxin-2/Ubiquitin conjugates in *Drosophila* eyes and S2 cells. a Volcano plot of proteins identified by mass spectrometry after biotin/streptavidin pulldowns from *Drosophila* adult heads expressing ^{bio}Ub (ubiquitin with biotinylation acceptor site) and Fbxo42 or Fbxl7, under the control of GMR-GAL4 driver. Results are presented as log_2 LFQ (label free quantitation) intensity ratios. As blue dots are ACC (acetyl-coenzyme A carboxylase) and PCB (pyruvate carboxylase), endogenous proteins which are biotinylated naturally and should have a log_2 ratio of around 0, if similar amount of biological samples have been isolated during the pulldown. Also as blue dots are Ubiquitin, Fbxl7 and Fbxo42. As green and red dots are proteins identified by at least 2 unique peptides, which are either enriched or depleted, respectively. Ataxin-2 (Atx2) is highlighted by a blue dashed circle. Statistical analysis was performed by two-sided Student's *t* test. The full results are provided in Supplementary Data 1. **b** Immunoblot from *Drosophila* adult heads expressing ^{bio}Ub, Fbxo42 and Ataxin-2-HA, under the control of GMR-GAL4 driver. *Drosophila* head lysates were subjected to biotin/streptavidin pull-downs and immunoblot with anti-HA. DTT sensitive Ataxin-2-HA ^{bio}Ub conjugates are detected by an upwards shift of the bands on the gel. $n = 3$ of biologically independent experiments.**c** Immunoblot of protein extracts from *Drosophila* S2 cells expressing His-myc-Ub, Ataxin-2-GFP and in the presence or absence of RNAi against Fbxo42. S2 cells lysates were subjected to Histidine (His) pulldown and immunoblots with anti-GFP (top panels) or anti-myc (bottom panels). DTT sensitive Ataxin-2-GFP His-myc-Ub conjugates are detected by an upwards shift of the bands on the gel and are not observed upon Fbxo42 RNAi treatment. * indicates residual His-myc-Ub-independent pulldown of Ataxin-2-GFP, presumably by direct interaction with the nickel resin. $n = 2$ of biologically independent experiments. Source data for figures (**b**, **c**) are provided as Source Data file. **d** Glossy eye phenotype caused by overexpression of Xbp1^{spliced} under the control of GMR-GAL4. Genotype: eyFlp,GMR-GAL4,UAS-Xbp1s/FM7. **e** Glossy eye phenotype is reduced in clones of Su218. Genotype: eyFlp,GMR-GAL4,UAS-Xbp1s; FRT42D, Su218/FRT42D, ubiGFP. **f** RNAi for Ataxin-2 suppresses the reduction of the "glossy" eye phenotype by clones of Su218. Genotype: eyFlp,GMR-GAL4,UAS-Xbp1s; FRT42D, Su218/FRT42D, ubiGFP; UAS-Ataxin-2 RNAi.

Supplementary Fig. 1h). The expected size for Fbxo42 is 74,4 kDa. This specific band is present in several 3rd instar larval tissues (Supplementary Fig. 1i) and in the adult brain, testis and ovaries (Supplementary Fig. 1j).

Fbxo42 promotes the formation of Ataxin-2-ubiquitin conjugates

In order to identify the specific substrate(s) of Fbxo42, we used a proteomic approach, based on the ^{bio}Ub strategy[15]. Transgenic flies with full-length FLAG-HA-Fbxo42, FLAG-HA-ΔFbxo42 or FLAG-Fblx7[16], a different F-box protein used as control, were crossed with ^{bio}Ub flies[15], a strain containing ubiquitin (Ub) with a short biotinylatable motif and BirA (biotin ligase), and GMR-GAL4, to drive the expression of the constructs in the *Drosophila* eye. We performed total protein extraction from FLAG-HA-Fbxo42, FLAG-HA-ΔFbxo42 and FLAG-Fblx7-expressing adult fly heads and confirmed expression of the F-box constructs and biotinylation of target proteins, by doing immunoblot with anti-FLAG and anti-Biotin antibodies (Supplementary Fig. 2a). To purify the ubiquitylated proteins, we performed pulldowns using a high-capacity streptavidin resin from triplicate samples, which were then processed for identification by mass spectrometry (MS) (Fig. 2a, Supplementary Fig. 2b and Supplementary Data 1). The values observed for the endogenously biotinylated acetyl-coenzyme A and pyruvate carboxylases (ACC and PCB) as well as for the overexpressed F-box proteins Fbxo42 and Fbxl7 (Fig. 2a) confirmed respectively that proportional amounts of biological material were isolated, and the overexpression of the corresponding F-box protein. In order to obtain results with statistical significance, stringent thresholds were established[15,17], to minimize the number of false positives. This approach led to the identification of Ataxin-2 as a Fbxo42 substrate, since Ataxin-2 is more ubiquitylated upon Fbxo42 overexpression, in comparison with Fbxl7 overexpression (Fig. 2a and Supplementary Data 1). Ataxin-2 is a RNA binding protein and participates in the formation of ribonucleoprotein granules[18].

To confirm the results obtained by mass spectrometry, we did immunoblots from biotin pulldowns of adult *Drosophila* head extracts expressing Ataxin-2-HA, ^{bio}Ub and FLAG-HA-Fbxo42 in the eye (GMR-GAL4). Ubiquitylated Ataxin-2-HA was observed as 2 bands of slower mobility in the gel, with the top band (orange arrow), but not the lower band (blue arrow), being sensitive to the presence of DTT (Dithiothreitol) in the elution buffer (Fig. 2b), an indication that Fbxo42 could be promoting the ubiquitylation of Ataxin-2 in one or more cysteines[19–21]. Furthermore, in *Drosophila* S2 cells, we could detect Ataxin-2-GFP/His-myc-Ubiquitin conjugates that were diminished upon the presence of DTT in the elution buffer or RNAi depletion of Fbxo42 (Fig. 2c). Importantly, RNAi depletion of Ataxin-2 abolished the suppression of Xbp1^{spliced}-induced glossy eye phenotype by Su218 (Fbxo42^{N423*}) (Fig. 2d–f), indicating that Ataxin-2 is a relevant substrate of Fbxo42 in the context of the assay that was used in the original genetic screen (Fig. 1). We confirmed the efficacy of the RNAi depletions of Fbxo42 in S2 cells (Supplementary Fig. 2c) and Ataxin-2 in *Drosophila* eyes (Supplementary Fig. 2d).

Fbxo42 interacts with Ataxin-2

To investigate further the interaction between Fbxo42 and Ataxin-2, we did co-immunoprecipitation (co-IP) assays from S2 cells (Fig. 3a) and *Drosophila* heads (Supplementary Fig. 3a) extracts. Ataxin-2-GFP can co-IP Fbxo42 in S2 cells (Fig. 3a) and FLAG-HA-Fbxo42 in *Drosophila* eyes (Supplementary Fig. 3a). These results were confirmed by immunofluorescence assays for Ataxin-2 and Fbxo42, using cells of the ring gland, the larval organ that synthetizes ecdysone and other hormones that control molting throughout development[22]. The cells of the ring gland are large, have polytene chromosomes and have endogenous activation of Ire1 signaling, confirmed by the expression of Xbp1s-GFP (Supplementary Fig. 3b), from a reporter of Ire1 activation, UAS-Xbp1-HA-GFP[23], where the Xbp1^{spliced} form is tagged with GFP and the unspliced form of Xbp1 (Xbp1^{unspliced}) is tagged with HA. Furthermore, ring gland cells express Ataxin-2 and Fbxo42 (Fig. 3b–f), and can easily be exposed to DTT, to induce high levels of ER stress and activation of the UPR. In untreated ring gland cells (Fig. 3b, c), Ataxin-2 and Fbxo42 have mostly uniform expression with little colocalization, although some Ataxin-2 granules are observed and Fbxo42 presents higher levels of expression in the corpus allatum than in the prothoracic gland (Fig. 3b). In ring glands treated with 5 mM DTT for 4 h (Fig. 3d–f), Ataxin-2 forms granules that are decorated with Fbxo42 foci (arrows in Fig. 3e and quantification in Fig. 3g). As an alternative method to induce the formation of Ataxin-2 granules in *Drosophila* cells, we used treatments with arsenite, as previously described[24]. Also in the case of arsenite treatments, we observed Fbxo42 foci decorating Ataxin-2 granules, both in the ring gland cells (Supplementary Fig. 3c) and in the follicle cells of the ovary (Supplementary Fig. 3d, e). Therefore, the recruitment of Fbxo42 to Ataxin-2 granules is not an exclusive of the induction of ER stress by DTT treatment.

Fbxo42 promotes the degradation of Ataxin-2

Often, ubiquitylated proteins are degraded by the proteosome[25]. To investigate whether ubiquitylation of Ataxin-2 by Fbxo42 promotes the degradation of Ataxin-2, we did cycloheximide (CHX) chase experiments in S2 cells. In these experiments, we probed the stability of Ataxin-2 by immunoblot after 0, 6 and 12 h of treatment of cells with CHX, an inhibitor of translation. Treating cells with CHX and MG132, an inhibitor of the proteosome, led to a significant stabilization of Ataxin-2-GFP (Supplementary Fig. 4a), an indication that Ataxin-2-GFP can be degraded by the proteosome. Next, we found that Fbxo42 overexpression promotes the degradation of Ataxin-2-GFP (Fig. 4a, b), while Fbxo42 RNAi depletion protects Ataxin-2-GFP from degradation (Fig. 4c, d). We confirmed these results by doing immunofluorescence

https://doi.org/10.1038/s41467-025-62417-2

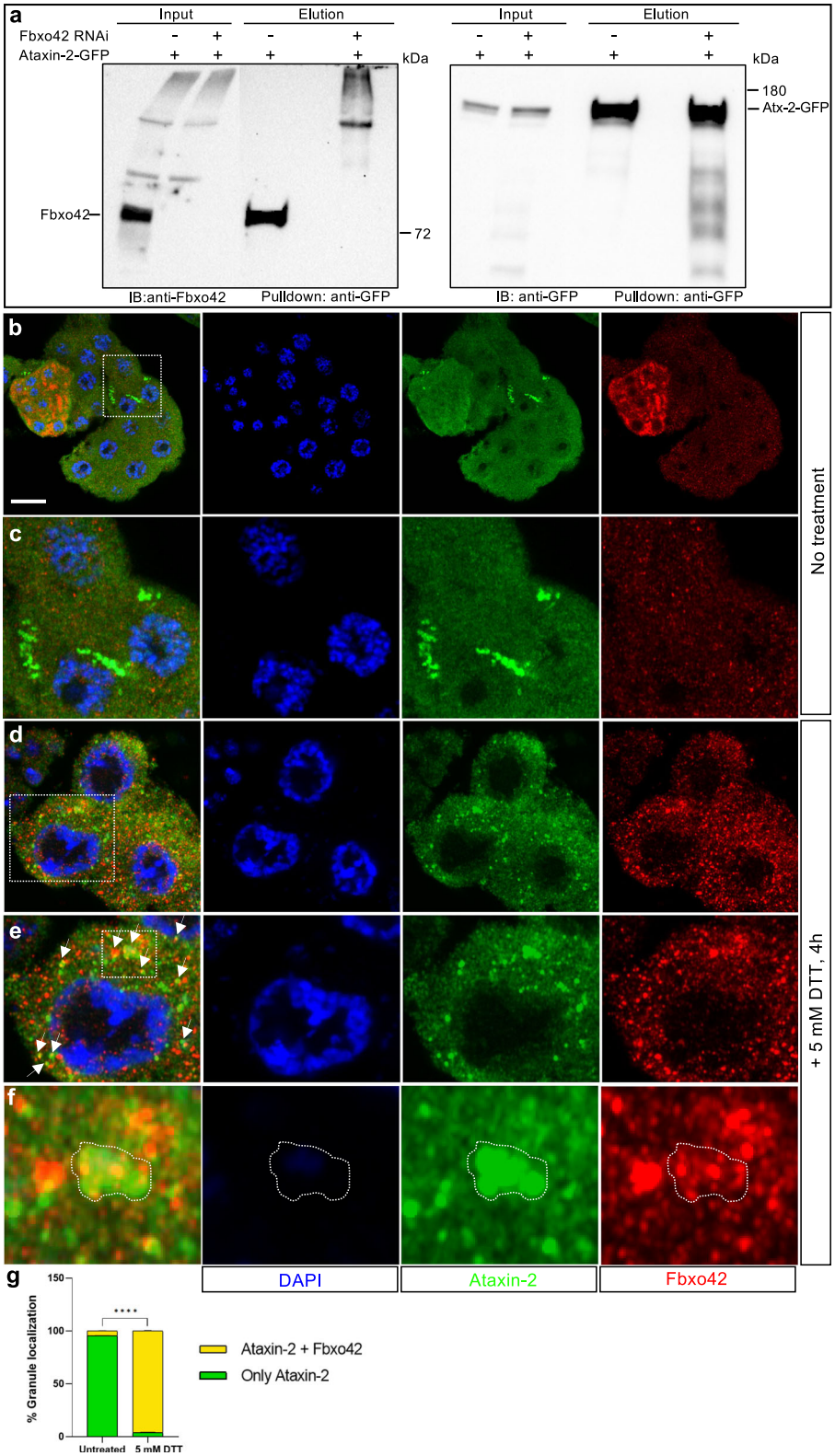

for Ataxin-2 in *Drosophila* 3rd instar larvae eye discs containing clones of cells homozygous for Su218 (Fbxo42^{N423*}), labelled by the absence of ubiGFP (Fig. 4e). Increased immunoreactivity for Ataxin-2 was observed in Fbxo42 homozygous mutant cells (highlighted by dashed lines and arrows in Fig. 4e), but only when the imaginal discs were treated with 5 mM DTT for 4 h, to induce ER stress, and only in the cells in the edge of the eye imaginal disc, presumably those exposed to higher amounts of DTT in the tissue.

To identify the cysteine residues in Ataxin-2 that are ubiquitylated upon overexpression of Fbxo42 we mutagenized C103, C154 or C244 to alanine (A) in Ataxin-2-GFP and did CHX chase experiments with these mutants, using S2 cells. While ataxin-2^{C244A}-GFP was stabilized (Fig. 4f, g), Ataxin-2^{C103A}-GFP and Ataxin-2^{C154A} -GFP (Supplementary Fig. 4b) presented profiles of protein degradation similar to WT Ataxin-2-GFP. Interestingly, in an Alphafold-3[26] prediction displaying the LSM and LSM-AD domains (amino acids 62–269) of Ataxin-2 together with a

Fig. 3 | Fbxo42 interacts with Ataxin-2 in *Drosophila* tissues and S2 cells. **a** Fbxo42 co-immunoprecipitates with Ataxin-2-GFP in S2 cells. Immunoblots probed with anti-Fbxo42 and anti-GFP antibodies from protein extracts of S2 cells expressing Ataxin-2-GFP before/after immunoprecipitation with anti-GFP beads and with/without Fbxo42 RNAi treatment. $n = 2$ of biologically independent experiments. **b** Immunofluorescence of ring gland (3rd instar larva) showing uniform staining of Ataxin-2 (green) and Fbxo42 (red). DAPI (blue) is a marker for nuclei. Scale bar = 30 µm. **c** Inset of (**b**). **d** Immunofluorescence of ring gland (3rd instar larva) after 4 h treatment with DTT (5 mM), to induce ER stress, shows Ataxin-2 (green) aggregates decorated with Fbxo42 (red). **e** Inset of (**d**). White arrows indicate examples of Ataxin-2 (green) aggregates decorated with Fbxo42 (red). **f** Inset of (**e**). Ataxin-2 granule (green), indicated with dashed line is decorated with several foci of Fbxo42 (red). **g** Quantification of the number of granules containing Ataxin-2 only (green bar) or Fbxo42-decorated Ataxin-2 granules (yellow bar) present in untreated ring gland cells (shown in (**b**)) and in ring gland cells treated with 5 mM DTT for 4 h (shown in (**d**)). The quantification was done in 2 biological replicates per condition and is presented in percentage (%) as mean ± SD. Two-way ANOVA coupled with Sidak's multiple-comparison test, $^{****}p < 0.0001$. The number of granules scored in untreated ring glands was $n = 277$ (replicate 1) and $n = 269$ (replicate 2). The number of granules scored in ring gland cells treated with DTT was $n = 552$ (replicate 1, from 15 cells) and $n = 523$ (replicate 2, from 11 cells). Source data for figures (**a**, **g**) are provided as Source Data file.

Fbxo42/Cullin-1/Skp-1/Rbx1/E2/Ub complex, C244 of Ataxin-2 localizes in the vicinity of the reactive C-terminus of Ub (Gly 76) and the catalytic Cys 85 of the E2 (Fig. 4h and Supplementary Fig. 4c). Furthermore, Ataxin-2^{C244A}-GFP did not present DTT-sensitive Ataxin-2-GFP/His-myc-Ubiquitin conjugates (Supplementary Fig. 4d). We conclude that Fbxo42 promotes the degradation of Ataxin-2 by mediating the ubiquitylation of the C244 residue. Experiments with human cell lines have shown that loss of Fbxo42 leads to cell cycle progression delays and aberrant mitosis[27], but the identity of the Fbxo42 substrates in this context remains unknown. Our results show that Fbxo42 is expressed in a variety of post-mitotic tissues, such as the ring gland or the developing *Drosophila* eye, and that Fbxo42 mediates the ubiquitylation and degradation of Ataxin-2 granules in these tissues.

Ataxin-2 binds the Xbp1 mRNA during UPR activation

To investigate further the regulatory link between the RNA binding protein Ataxin-2 and Xbp1, we asked whether Ataxin-2 and Xbp1 mRNA could co-localize in cells undergoing activation of the UPR. We performed immunostaining with anti-Ataxin-2 and RNA fluorescent in situ hybridization (FISH) for Xbp1 mRNA in ring gland cells of *Drosophila* larvae treated with DTT, to induce high levels of UPR activation. In cells with no DTT treatment, Xbp1 mRNA is mostly detected in the cytoplasm, with little colocalization with Ataxin-2 (Fig. 5a). In DTT treated cells, Xbp1 mRNA colocalizes with cytoplasmic Ataxin-2 granules (arrows in Fig. 5b and quantification in Fig. 5c). Ataxin-2 is not present in Xbp1 mRNA nuclear foci (arrowheads in Fig. 5b) that presumably correspond to Xbp1 transcription, since it is known that Xbp1 transcription is induced by ER stress and UPR activation[28]. To assess the specificity of our Xbp1 mRNA FISH probes, we used eye imaginal discs containing clones of Ex250[29,30], a deletion of most of *Xbp1*, that show strongly reduced FISH signal of Xbp1 mRNA in the Ex250 homozygous clones (Supplementary Fig. 5a).

These results suggest that, during UPR activation, Ataxin-2 binds to Xbp1 mRNA, which is found in cytoplasmic Ataxin-2 granules. To identify Ataxin-2 binding sites in the Xbp1 mRNA, we performed iCLIP (individual-nucleotide resolution UV crosslinking and immunoprecipitation)[31] in S2 cells transfected with Ataxin-2-HA and treated with DTT (5 mM, 4 h), to induce high levels of UPR activation. Using an improved iCLIP protocol[32], we found that Ataxin-2 binds to several sites in the Xbp1 mRNA, and specifically to a region of the 3'UTR containing an AU-rich motif (Fig. 5d, Supplementary Fig. 5b, c), which is consistent with the binding specificity previously identified for human and *Drosophila* Ataxin-2[33,34]. We also performed iCLIP experiments in S2 cells upon ectopic expression of Ataxin-2^{C244A}, the point mutation that protects Ataxin-2 from Fbxo42-mediated ubiquitylation and degradation. Interestingly, although Ataxin-2^{C244A} binds the Xbp1 mRNA, there is a reduction in the number of iCLIP crosslinks, perhaps because C244 is in the LSM-AD domain that is involved in RNA binding and is essential to rescue the lethality of Ataxin-2 trans-heterozygous mutations[35]. Motif analysis around Ataxin-2 crosslink sites showed that various AU-rich pentamers (with a 'C' or 'G' or without) were enriched at the transcriptomic level in both wild-type and mutant Ataxin-2, but not in samples that were not UV-crosslinked (Supplementary Fig. 5b). Moreover, the iCLIP crosslink positions (i.e. start positions of iCLIP cDNAs) were directly aligned with the motif centers at the metagene level (Supplementary Fig. 5c), including the GUUUC pentamer that was bound by Ataxin-2 on the Xbp1 3'UTR (Supplementary Fig. 5c).

Finally, we confirmed our findings in human (HeLa) cells (Supplementary Fig. 5d–f), where we also found co-localization of Xbp1 mRNA with Ataxin-2 in cells exposed to thapsigargin (Tg, 1 µM) or sodium arsenite (SA, 500 µM), during 2 h.

Ataxin-2 stabilizes Xbp1 mRNA

To test whether Ataxin-2 regulates the stability of Xbp1 mRNA, we performed actinomycin D (ActD) chase experiments in S2 cells, using the Xbp1 reporter for Ire1 activation, where the Xbp1^{spliced} form is tagged by GFP[5,23]. After ER stress induction with DTT (for 4 h) and transcription inhibition with actinomycin D, the decay of the Xbp1 reporter mRNA was analyzed over time in S2 cells treated either with Ataxin-2 RNAi or control LacZ RNAi. Upon Ataxin-2 depletion, the stability of the Xbp1 reporter mRNA is decreased in comparison with the LacZ RNAi control condition (Fig. 6a). This result was confirmed by immunoblotting experiments (Fig. 6b, c), showing that, upon Ataxin-2 depletion and after DTT treatment (5 mM, 4 or 8 h), the levels of Xbp1^{spliced}-GFP protein are decreased in comparison with the LacZ RNAi control condition. Taken together, these results show that Ataxin-2 promotes Xbp1 mRNA stabilization and more Xbp1^{spliced} protein expression during UPR activation, being consistent with the results that show that human Ataxin-2 (ATXN-2), in general, stabilizes its target mRNAs and increases the abundance of the corresponding proteins (Yokoshi et al., 2014).

Fbxo42 releases XBP1s mRNA from Ataxin-2 granules, allowing for its translation under stress conditions

Finally, we did immunoblotting experiments (Fig. 6d, e), showing that, upon Fbxo42 depletion and after DTT treatment (5 mM, 4 or 8 h), the levels of Xbp1^{spliced}-GFP protein are decreased in comparison with the LacZ RNAi control condition. Likewise, expression of Xbp1s-GFP is reduced in clones of cells that are homozygous for Su218 (Fig. 6f), which is consistent with the results obtained from the genetic screen, where loss-of-function mutation in Fbxo42 led to the suppression of the glossy eye phenotype caused by overexpression of Xbp1s. These results suggest that Fbxo42 mediated degradation of Ataxin-2 is required for the release of XBP1s mRNA from Ataxin-2 granules, thus allowing for the translation of the XBP1s mRNA under stress conditions.

Discussion

In this study, we performed a genetic screen for suppressors of Xbp1^{spliced} induced "glossy" eye phenotype, leading to the identification of loss-of-function mutations in Fbxo42. Subsequently, we did a ^{bio}Ub pulldown/proteomic experiment to identify Fbxo42 substrates, which led to the identification of Ataxin-2. Fbxo42 is recruited to Ataxin-2 granules during the activation of the UPR to ubiquitylate and promote the degradation of Ataxin-2. We show that Ataxin-2 binds to and stabilizes Xbp1 mRNA during the activation of the UPR, and that

https://doi.org/10.1038/s41467-025-62417-2

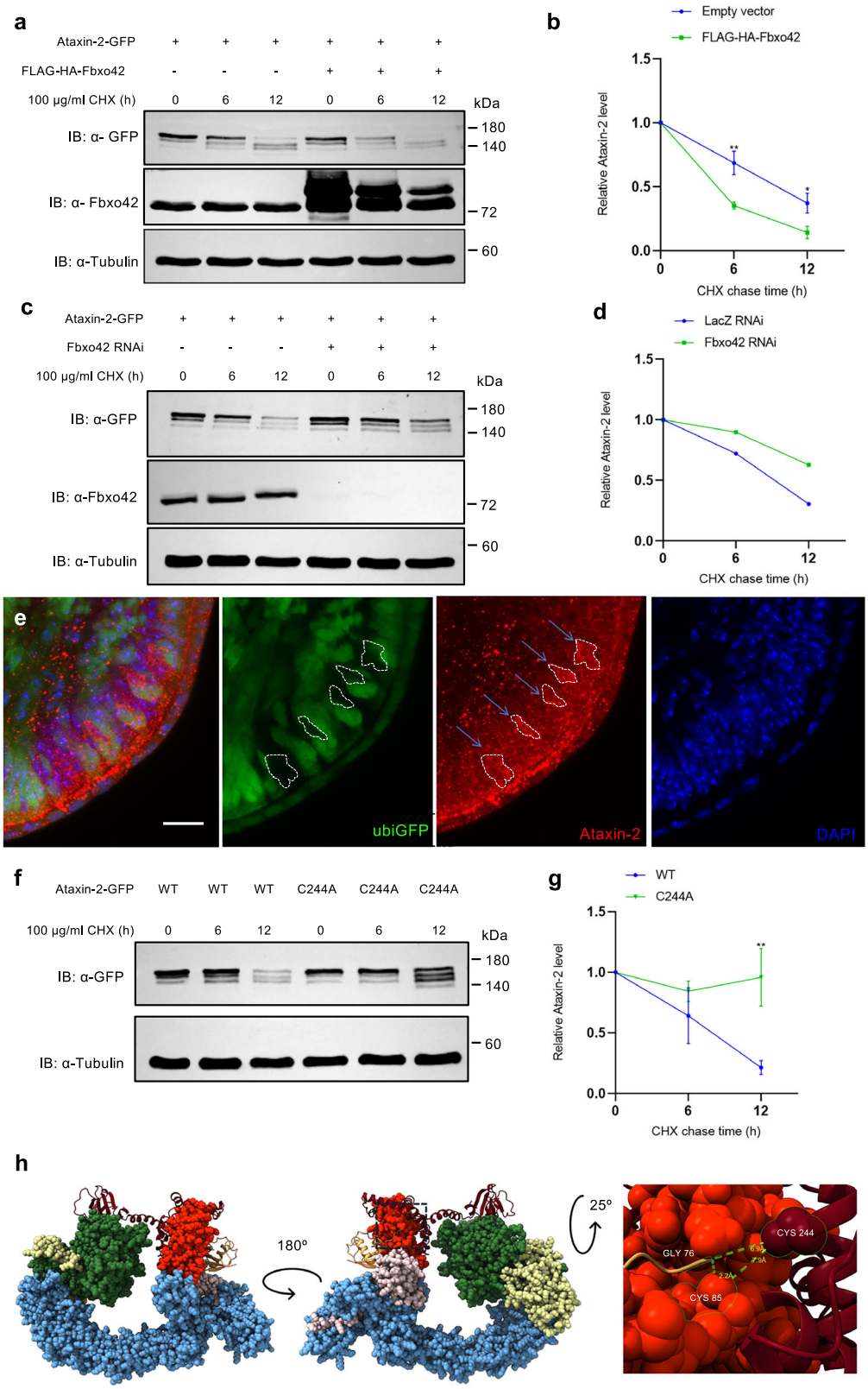

degradation of Ataxin-2 granules by Fbxo42 is required for the accumulation of Xbp1^{spliced} protein.

We summarize these findings in a model in Fig. 7. Upon high levels of ER stress, Xbp1 mRNA is spliced by the endoribonuclease activity of Ire1 and goes to Ataxin-2 granules, where it is protected from degradation but not translated. Polysome profiling experiments have shown that Ataxin-2 is found predominantly in non-ribosomal fractions[33] and therefore, Ataxin-2-bound mRNAs are predominantly not translated. The progressive recruitment of Fbxo42 to Ataxin-2 granules leads to the ubiquitylation and degradation of Ataxin-2, releasing the Xbp1 mRNA free to be translated. In Fbxo42 mutant cells, Xbp1 mRNA remains not translated in Ataxin-2 granules, with less Xbp1 signaling readout (glossy eye phenotype), as in our initial genetic screen (Fig. 1).

Fig. 4 | Fbxo42 promotes the degradation of Ataxin-2. a Immunoblots probed with anti-Fbxo42 and anti-GFP antibodies from protein extracts of *Drosophila* S2 cells expressing Ataxin-2-GFP and FLAG-HA-Fbxo42 or Ataxin-2-GFP and empty vector negative control. S2 cells were treated with cycloheximide to inhibit protein translation and protein extracts were "chased" at the indicated time points. Tubulin was used as loading control and it was detected on the same membrane as Ataxin-2-GFP and Fbxo42. **b** Quantification of Ataxin-2-GFP protein levels from (**a**) and 2 other biologically independent experiments ($n = 3$) is presented as mean ± SEM. Two-way ANOVA coupled with Sidak's multiple-comparison test, $^{**}p = 0.0027$ at 6 h for Ataxin-2-GFP+empty vector (blue circles) vs Ataxin-2-GFP+FLAG-HA-Fbxo42 (green squares); $^{*}p = 0.0322$ at 12 h for Ataxin-2-GFP+empty vector vs Ataxin-2-GFP +FLAG-HA-Fbxo42. **c** Immunoblots probed with anti-Fbxo42 and anti-GFP antibodies from protein extracts of *Drosophila* S2 cells expressing Ataxin-2-GFP and Fbxo42 RNAi or Ataxin-2-GFP and LacZ RNAi, as negative control. S2 cells were treated with cycloheximide to inhibit protein translation and protein extracts were "chased" at the indicated time points. Tubulin was used as loading control and it was detected on the same membrane as Ataxin-2-GFP. **d** Quantification of Ataxin-2-GFP protein levels from **c** and 1 other biologically independent experiment ($n = 2$) is presented as mean ± SEM, where Ataxin-2-GFP+Fbxo42 RNAi is represented by green squares and Ataxin-2-GFP+LacZ RNAi is represented by blue circles. **e** Immunofluorescence of 3rd instar larva eye discs containing clones of Su218, labelled by the absence of ubiGFP (green). Endogenous Ataxin-2 is in red and DAPI (blue) is a marker for nuclei. Whole brain/eye disc tissues were treated with 5 mM DTT (in PBS) for 4 h, before fixation with formaldehyde. Genotype: eyFlp, GMR-GAL4; FRT42D, Su218/FRT42D, ubiGFP. Scale bar = 10 µm. **f** Immunoblots probed with anti-GFP from protein extracts of *Drosophila* S2 cells expressing Ataxin-2-GFP or Ataxin-2^{C244A}-GFP. S2 cells were treated with cycloheximide to inhibit protein translation and protein extracts were "chased" at the indicated time points. Tubulin was used as loading control and it was detected on the same membrane as wild-type and mutant Ataxin-2-GFP. **g** Quantification of Ataxin-2-GFP (WT, blue circles) and Ataxin-2^{C244A}-GFP (green triangles) protein levels from **f** and 2 other biologically independent experiments ($n = 3$) is presented as mean ± SEM. Two-way ANOVA coupled with Sidak's multiple-comparison test, $^{**}p = 0.0087$ at 6 h for wild-type Ataxin-2-GFP vs Ataxin-2^{C244A}-GFP. **h** Alphafold-3 prediction of a complex containing the LSM and LSM-AD domains (N57 to Q270) of Ataxin-2 (oxblood) together with Fbxo42 (green), Skp1 (yellow), Cullin1 (light blue), Rbx1 (pink), E2-ubiquitin conjugating enzyme (Effete, red) and Ubiquitin (Ub, orange). All proteins are represented as spheres except for Ataxin-2 and Ub that are in ribbon view. The right panel is a zoom in the region highlighted by the black dashed rectangle, with a green highlight in Cys 244 of Ataxin-2, the catalytic Cys 85 of the E2 (Effete) and the reactive C-terminus of Ub (Gly 76). Source data for figures (**a**–**d**) and (**f**–**h**) are provided as Source Data file.

The model in Fig. 7 is largely inspired by the results from the Ataxin-2/Fbxo42 immunofluorescence and Xbp1 mRNA FISH/Ataxin-2 immunofluorescence experiments (Figs. 3 and 5). Although the Xbp1 mRNA FISH probes do not distinguish Xbp1^{spliced} from Xbp1^{unspliced}, these experiments were done after 4 h of exposure of the tissues to DTT, when most Xbp1 mRNA is already spliced by Ire1, but Xbp1s translation is still reduced[36,37]. In mouse embryonic fibroblasts, Xbp1s protein levels show a gradual increase between 3 and 9 h of treatment with the ER stress inducer thapsigargin[36], which is consistent with our studies in *Drosophila* S2 cells, where we typically see the highest levels of Xbp1s-GFP protein only upon 8 h of DTT treatment (Fig. 6b, d and ref. 23). Our present results explain this temporal delay between the availability of Xbp1^{spliced} mRNA and the emergence of Xbp1^{spliced} protein – the Xbp1 mRNA stays untranslated in Ataxin-2 granules during the first few hours of ER stress and UPR activation.

Importantly, in ring gland cells, Ire1 signaling is activated even in the absence of DTT treatments (Supplementary Fig. 3b), perhaps as part of their developmental role in the biosynthesis and secretion of the ecdysone hormone. However, the strong co-localization of Xbp1 mRNA with Ataxin-2 granules in ring gland cells only occurs upon DTT treatment and is concomitant with the strong transcriptional activation of Xbp1 (Fig. 5b). Therefore, regulation of Xbp1 mRNA by Ataxin-2 could be important only when the UPR activation leads to very high levels of Xbp1 transcription, for example by exposure of cells to DTT or overexpression of Xbp1^{spliced}, as in our original genetic screen (Fig.1).

Cell death receptors (CD or DR) play a pivotal role in ER stress-induced cell death, including DR5[38] and CD95[39]. While the Ire1 RNase activity degrades the mRNAs of DR5[38] and CD95[39] during an early, adaptative pro-survival stage (up to 6 h of ER stress), the expression of DR5 and CD95 is upregulated at later stages, committing cells to the death fate. In this context, Xbp1s activates the transcription of CD95 to kill cells[39]. Therefore, while the mRNA of Xbp1 progressively accumulates in Ataxin-2 granules during the early, adaptative pro-survival stages, at later stages this large storage of Xbp1 mRNA could be quickly translated, upon the degradation of Ataxin-2 by Fbxo42, to trigger the transcriptional activation of cell death receptors and kill cells.

Methods

Plasmids

The cDNA clone GH02866 [*Drosophila* Genomics Resource Center (DGRC), DGRC Stock 6307; https://dgrc.bio.indiana.edu//stock/6307; RRID: DGRC_6307] was used to clone *Fbxo42* into the Gateway® destination vectors pTFHW (to generate a N-terminally 3xFLAG-3xHA-tagged fusion protein) and pTWG (to create a C-terminally GFP-tagged fusion protein) following Invitrogen Gateway® protocol (Invitrogen). Primers used to generate pTFHW-Fbxo42 and pTWG-Fbxo42 are listed in Supplementary Table 1.

The pTFHW-ΔFbxo42 vector contains the deletion of the first 201 base pairs of *Fbxo42* gene. This region encodes the first 67 amino acids of Fbxo42, and it includes the F-box domain. Δ*Fbxo42* sequence was cloned into the Gateway® destination vector pTFHW (primers in Supplementary Table 1).

The pUAST-Ataxin-2-GFP construct was generated by Gibson Assembly® (New England Biolabs, NEB). Briefly, the *Ataxin-2* gene was amplified by PCR from flies expressing Ataxin-2 isoform A C-terminally fused with HA-tag (FlyORF F001031) and subcloned into the pJET1.2/blunt vector (CloneJET™ PCR Cloning Kit, Fermentas/Thermo Fisher Scientific), generating the pJET1.2-Ataxin-2-HA construct. Afterwards, the *Ataxin-2* sequence was PCR amplified from pJET1.2-Ataxin-2-HA and *gfp* was amplified from pUAST-Xbp1-EGFP (primers in Supplementary Table 1). Finally, the Ataxin-2 and GFP DNA fragments were cloned into the pUAST vector at XhoI (Fermentas/Thermo Fisher Scientific)/BglII (Thermo Fisher Scientific) restriction sites by Gibson reaction.

To generate the pUAST-Ataxin-2-HA construct, the DNA sequence encoding Ataxin-2 C-terminally fused with HA-tag was PCR amplified (primers in Supplementary Table 1) from pJET1.2-Ataxin-2-HA vector and cloned into pUAST plasmid at XhoI/BglII restriction sites by Gibson Assembly®.

The *Ataxin-2* mutations were generated by site-directed mutagenesis using the NZYMutagenesis kit (NZYtech) according to the manufacturer's instructions. All plasmid constructs were confirmed by sequencing (Stabvida). The pUAST-His-Myc-Ubiquitin plasmid[40] was kindly provided by HD Ryoo. The pMT-SkpA-HA and UAS-FLAG-Fblx7[16] plasmids were a gift from Iswar Hariharan.

Drosophila stocks

Fly stocks and crosses were raised with standard cornmeal fly food, at 25 °C under 12 h light/12 h dark cycles. New transgenic fly lines were made either at Bestgene or the Champalimaud Foundation transgenics facility. The fly stocks UAS-Xbp1u[41], UAS-Xbp1s[5], UAS-P35[42], UAS-DIAP1[43] and UAS-Rh1[11] were gifts from Hyung Don Ryoo. The stock GMR-hid, eyFlp[44] was a gift from Andreas Bergmann. The stock UAS-FLAG-Fblx7[16] was a gift from Iswar Hariharan.

To identify the Fbxo42 substrates by mass spectrometry, flies bearing on the second chromosome a polyubiquitin chain conjugated

https://doi.org/10.1038/s41467-025-62417-2

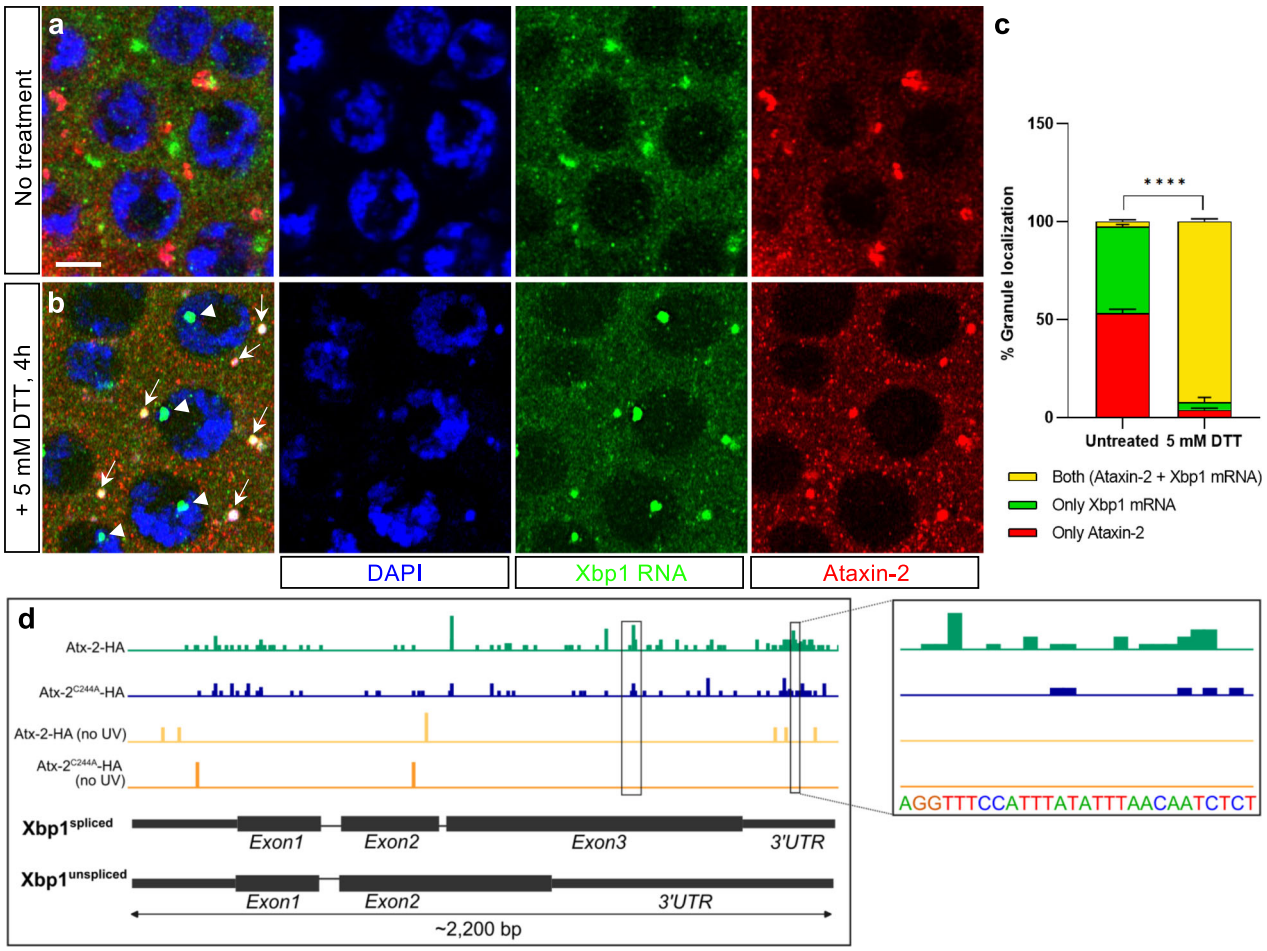

Fig. 5 | Ataxin-2 binds Xbp1 mRNA during UPR activation. **a** Immunofluorescence and RNA FISH of untreated ring gland cells (3rd instar larva). Endogenous Ataxin-2 is in red (anti-Ataxin-2 antibody), Xbp1 mRNA in green (Stellaris FISH probes against Xbp1) and the nuclei is in blue (DAPI). Scale bar = 10 µm. **b** Immunofluorescence and RNA FISH of ring gland cells treated with 5 mM DTT (to induce ER stress and UPR activation) for 4 h. Endogenous Ataxin-2 (red), Xbp1 mRNA (green) and nuclei (blue), as in (**a**). Arrows indicate Xbp1 mRNA in Ataxin-2 granules. Arrowheads indicate Xbp1 mRNA in the nucleus. **c** Quantification of the number of granules of Ataxin-2 protein only (red bar), Xbp1 mRNA only (green bar) or both Ataxin-2 protein and Xbp1 mRNA (yellow bar), in untreated ring gland cells (shown in (**a**)) and in ring gland cells treated with 5 mM DTT for 4 h (shown in (**b**)). The quantification was done in 2 biological replicates per condition and is presented in percentage (%) as mean ± SD. Two-way ANOVA coupled with Sidak's multiple-comparison test, $^{****}p < 0.0001$. The number of granules scored in untreated ring glands was $n = 125$ (replicate 1) and $n = 150$ (replicate 2). The number of granules scored in ring gland cells treated with DTT was $n = 123$ (replicate 1) and $n = 156$ (replicate 2). **d** iCLIP results for Xbp1/Ataxin-2-HA. In green are depicted the peaks (sequencing reads) in *Xbp1* from UV-irradiated S2 cells transfected with Ataxin-2-HA. In blue are depicted the peaks in *Xbp1* of UV-irradiated cells transfected with Ataxin-2^{C244A}-HA. The non-UV irradiated controls for Ataxin-2-HA and Ataxin-2^{C244A}-HA samples are shown by the yellow and orange lines, respectively. To the right is a zoom of the *Xbp1* 3'UTR containing the AU-rich region.

with biotin and fused with *E.coli* BirA (biotin ligase), UAS-(^{bio}Ub)$_6$-BirA[15], were crossed with flies carrying on the third chromosome the full-length Fbxo42 N-terminally tagged by 3xFLAG-3xHA-tag or the F-box control constructs: UAS-3xFLAG-3xHA-ΔFbxo42 (containing the deletion of the F-box domain) or UAS-FLAG-Fbxl7 (carrying a different fly F-box protein). Flies containing UAS-3xFLAG-3xHA-Fbxo42 without UAS-(^{bio}Ub)$_6$-BirA were used as an additional control. The constructs were expressed in the *Drosophila* eye using the Glass Multimer Reporter-GAL4 driver (GMR-GAL4).

To confirm the mass spectrometry results, virgin female flies from the GMR-GAL4, UAS-(^{bio}Ub)$_6$-BirA; UAS-FLAG-HA-Fbxo42 stock were crossed with male flies overexpressing Ataxin-2 isoform A C-terminally fused with 3xHA-tag (UAS-Ataxin-2-HA), obtained from FlyORF – Zurich ORFeome Project (fly line ID: F001031).

For the GFP pulldowns using fly heads, virgin female flies from GMR-GAL4, UAS-(^{bio}Ub)$_6$-BirA; UAS-FLAG-HA-Fbxo42 or GMR-GAL4, UAS-(^{bio}Ub)$_6$-BirA; UAS-FLAG-Fbxl7 stocks were crossed with male flies bearing UAS-Ataxin-2-GFP construct on the second chromosome.

Mutant clones in eye imaginal discs were generated by FLP (flippase recombinase)/FRT (FLP recombination target) recombination system[8], where flippase expression is under the control of the *eyeless* (*ey*) promoter.

To express Ataxin-2 RNAi in Xbp1s-induced "glossy eye" with Fbxo42 mutant suppressor clones, female flies carrying one of the Fbxo42 suppressors, FRT42D, Su218 (Fbxo42^{N423*}) were crossed with male flies bearing UAS-Ataxin-2 RNAi (BL 36114). Males from the progeny containing FRT42D, Su218 and UAS-Ataxin-2 RNAi were crossed with female flies with the genotype eyFlp, GMR-GAL4, UAS-Xbp1^{spliced}; FRT42D, ubiGFP. Flies bearing eyFlp, GMR-GAL4, UAS-Xbp1^{spliced}; FRT42D, Su218/ FRT42D, ubiGFP without UAS-Ataxin-2 RNAi were used as control.

Mosaic genetic screen and mapping

The FRT42D stock was isogenized and males were collected for ethyl methanesulfonate (EMS) treatment. The males were starved for 8 h in empty plastic vials and fed with a 25 mM EMS solution overnight for 16–18 h (paper tissue soaked with EMS solution on the bottom of the

https://doi.org/10.1038/s41467-025-62417-2

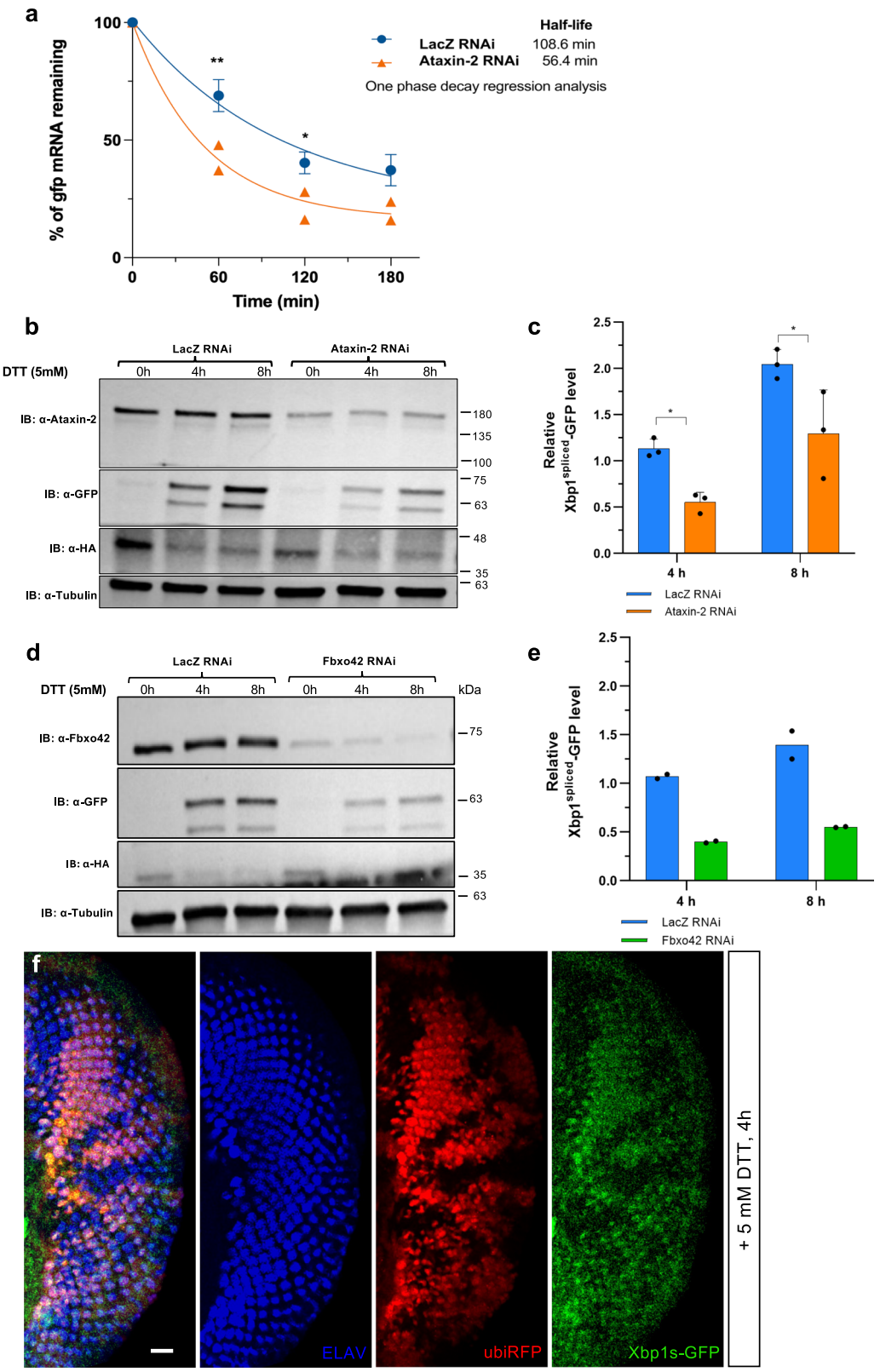

vials). After EMS treatment, around 60 males were given one hour for recovery on tissue paper and were then crossed in mass to around 150 virgins of the genotype eyFlp, GMR-GAL4, UAS-Xbp1^{spliced}; FRT42D, ubiGFP. The crosses were settled in new bottles every day, for four days in total and the F1 generation was screened for mosaic clones with suppression of the "glossy" eye phenotype. Suppressors of the "glossy" eye phenotype were balanced over CyO and retested for a reproducible phenotype. Only suppressor stocks that were homozygous lethal were kept, which was necessary for mapping of the mutations. For complementation analysis, each suppressor stock obtained from the screen was crossed to each other to bring the mutations in trans in the progeny to analyze whether unbalanced flies or flies only with the balancer CyO existed. When only CyO balanced progeny existed, the two suppressor mutations are lethal in trans and

Fig. 6 | Ataxin-2 and Fbxo42 regulate the stability and translation of Xbp1 mRNA during UPR activation. a Actinomycin D (ActD) chase experiments using S2 cells treated with Ataxin-2 RNAi (orange triangles) or LacZ RNAi (control, blue circles) and transfected with pUASTattb-Xbp1-HA-GFP. The cells were treated with 5 mM DTT (for 4 h), to induce ER stress, and subsequently incubated with 5 µg/ml ActD until the indicated chase time points. Data are presented as mean ± SD of % of *gfp* mRNA remaining, normalized to *rp49* from biologically independent experiments: LacZ RNAi $n = 3$ and Ataxin-2 RNAi $n = 2$. Half-life for each treatment was calculated by one phase regression analysis (R^2 LacZ RNAi = 0.9459; R^2 Ataxin-2 RNAi = 0.9560). Statistical significance was determined for each point: 60 min, $p^{**} = 0.026$; 120 min, $p^{*} = 0.047$; 180 min, $p = 0.057$. **b** Immunoblot of $Xbp1^{spliced}$-GFP (probed with anti-GFP), $Xbp1^{unspliced}$-HA (probed with anti-HA) and Ataxin-2 (probed with anti-Ataxin-2) after 5 mM DTT incubation for 0, 4 and 8 h. Tubulin was used as loading control and it was detected on the same membrane as XBP1 and Ataxin-2-HA. S2 cells were treated with LacZ RNAi or Ataxin-2 RNAi and transfected with Xbp1-HA-GFP. **c** Quantification of $Xbp1^{spliced}$-GFP protein levels from (**b**) and 2 other biologically independent experiments ($n = 3$) is presented as mean ± SD. Two-way ANOVA coupled with Sidak's multiple-comparison test, $^{*}p = 0.0496$ at 4 h for S2 cells treated with LacZ RNAi and expressing $Xbp1^{spliced}$-GFP (blue bar) vs S2 cells treated with Ataxin-2 RNAi and expressing $Xbp1^{spliced}$-GFP (orange bar); $^{*}p = 0.0150$ at 8 h for S2 cells treated with LacZ RNAi and expressing $Xbp1^{spliced}$-GFP vs S2 cells treated with Ataxin-2 RNAi and expressing $Xbp1^{spliced}$-GFP. **d** Immunoblot of $Xbp1^{spliced}$-GFP (probed with anti-GFP), $Xbp1^{unspliced}$-HA (probed with anti-HA) and Fbxo42 (probed with anti-Fbxo42) after 5 mM DTT incubation for 0, 4 and 8 h. Tubulin was used as loading control and it was detected on the same membrane as XBP1 and Fbxo42. S2 cells were treated with LacZ RNAi or Fbxo42 RNAi and transfected with Xbp1-HA-GFP. **e** Quantification of $Xbp1^{spliced}$-GFP protein levels from (**d**) and 1 other independent experiment is presented as mean ± SD. **f** Immunofluorescence of 3rd instar larva eye discs containing clones of Su218, labelled by the absence of ubiRFP (red), Xbp1s-GFP is in green and the photoreceptor marker ELAV is in blue. The larval discs were treated with 5 mM DTT for 4 h before fixation to activate Ire1-mediated splicing of Xbp1-HA-GFP. Scale bar = 10 µm. Genotype: eyFlp,GMR-GAL4; FRT42D,ubiRFP/ FRT42D,Su218; UAS-Xbp1-HA-GFP.

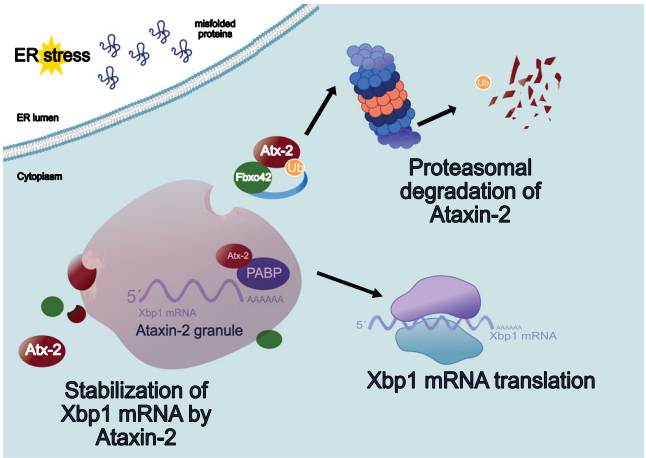

Fig. 7 | Model of Xbp1 mRNA regulation by Ataxin-2 and Fbxo42. Upon ER stress, Xbp1 mRNA is transcribed and progressively accumulates in Ataxin-2 (Atx-2) granules, where it is protected from degradation. Ataxin-2 binds Xbp1 mRNA, together with Poly(A)-binding protein (PABP). Fbxo42 binds to Ataxin-2, promoting the ubiquitylation (Ub) of Ataxin-2 and its degradation by the proteosome. Xbp1 mRNA is released from Ataxin-2 granules and is translated by the ribosome.

likely have a lethal hit in the same gene. For mapping of the suppressor mutations, we used the 2R deficiency kit (from the Bloomington *Drosophila* Stock Center). Virgins of the suppressor mutations balanced over CyO were crossed to males of each of the stocks bearing the balanced deficiencies and the F1 generation was screened for trans-heterozygosity. The existence of only balanced flies in F1 generation, indicated that the mutation is located within the region of the deficiency. The process was repeated with other smaller deficiencies until it could be defined the smallest region harboring the suppressor mutation. When available, we then tested lethal mutations in candidate genes in the region for trans-lethality with our mutations. The molecular identification of the mutations was done by genomic DNA sequencing of candidate genes from larvae homozygous for the suppressor mutations, collected from stocks balanced over CyO-GFP and also from the parental FRT42D stock before EMS mutagenesis. Genomic DNA preparation was done with the High Pure PCR Template Preparation kit from Roche and sequencing was performed by Stabvida.

Anti-Fbxo42 antibody generation

To generate the anti-Fbxo42 rabbit polyclonal antibody, the DNA sequence coding for amino acids 384–667 of Fbxo42 was cloned into pETM-30 at XhoI/NcoI (NEB) restriction sites, to generate a N-terminal GST tagged protein. Beyond GST, Fbxo42 was tagged with two Histine (His)-tags placed on N- and C- terminals. Protein expression was performed in Rosetta bacterial cells. Supernatant and pellet extracts were run in 8% SDS-PAGE gels. Fbxo42 was purified by His-tag using a resin containing nickel [Profinity™ IMAC (Immobilized-Metal Affinity Chromatography) Ni-Charged Resin (cat. no. 156-0131, Bio-Rad)]. The purified Fbxo42 antigen in solution was sent to Eurogentec for antibody production, with subsequent in gel affinity purification of the antibody being performed in the laboratory. To minimize the background staining in immunofluorescence and immunoblot experiments, affinity purified anti-Fbxo42 antibody was preabsorbed with L1 larvae homozygous for Su226 ($Fbxo42^{H436^{*}}$).

Immunofluorescence and imaging

Drosophila adult or larval tissues were dissected in 1× PBS, fixed with 4% PFA (paraformaldehyde) in 1× PBS at room temperature for at least 45 min and washed three times with PBT (1× PBS + 0.3% Triton X-100), 10 min each. Afterwards, fly's tissues were incubated with primary antibodies diluted in BBT-250 (0.1% BSA, 0.1% Triton X-100, 250 mM NaCl in 1× PBS) overnight, at 4 °C under gentle agitation. The primary antibodies used were as follow: rat anti-ELAV (1:200, 7E8A10, Developmental Studies Hybridoma Bank, DSHB), guinea-pig anti-Ataxin-2[45] (1:200, a kind gift from Patrick Emery), mouse anti-HA (1:200, Covance, MMS101P) and rabbit anti-Fbxo42 (1:100). Incubation with anti-Fbxo42 antibody was preceded by an extra step of blocking and permeabilization; tissues were incubated in block-permeabilization solution (1% BSA, 0.3% Triton X-100 in 1× PBS) for 1 h at room temperature. After overnight incubation with primary antibodies, fly's tissues were washed three times with PBT for 10 min each and incubated with fluorescent conjugated secondary antibodies (Jackson ImmunoResearch Laboratories) for 2 h at room temperature. Following three washes in PBT, the tissues were mounted in VECTASHIELD® Antifade Mounting Medium with DAPI (Vector Laboratories, H-1200-10) and image acquisition was performed on a confocal microscope (Leica SP5 Live or Zeiss LSM 880). Typically, sixty eye imaginal discs were dissected, and at least ten images were acquired for each genotype. For imaging of adult fly eyes, 2–5 days old flies were anesthetized with CO_2 and transferred to a microscope slide where fly bodies were immobilized with transparent nail polish. *Drosophila* eye' s pictures were acquired using a Leica Z16 APO macroscope equipped with a Leica DFC 420C camera with Leica's extended depth of focus (Montage) software.

To promote UPR activation and the formation of Ataxin-2 granules, larval tissues were exposed to 5 mM DTT for 4 h in PBS. As an alternative method to induce the formation of Ataxin-2 granules, larval tissues were treated with 0.5 mM arsenite for 2 hours. Untreated larval tissues were used as control.

Adult ovaries were dissected in 1× PBS and then transferred to Schneider's *Drosophila* medium (Biowest). Ataxin-2 granules were induced by incubating ovaries with 0.5 mM arsenite in Schneider's medium for 2 h at 25 °C[46]. Untreated ovaries were kept in Schneider's medium and used as control.

^{bio}Ub pulldowns

For the biotin pulldowns were used the aforementioned fly stocks carrying GMR-GAL4, UAS-(^{bio}Ub)$_6$-BirA together with one of the following F-box constructs: UAS-FLAG-HA-Fbxo42; UAS-FLAG-HA-ΔFbxo42 or UAS-FLAG-Fbxl7, the latter two used as controls. Flies bearing only UAS-FLAG-HA-Fbxo42 without ^{bio}Ub or BirA were used as an additional control. Adult flies with 2–5 days old were collected and fragmented by several rounds of flash freezing in liquid nitrogen and vortexing. Afterwards, fly heads were separated from the remaining body parts using a set of sieves with a nominal cut-off of 850, 710 and 425 μm on dry ice. Biotin pull-downs from *Drosophila* heads were performed as previously described[15]. Briefly, 500 mg of fly heads from each genotype was homogenized in 2.9 ml of lysis buffer (8 M urea, 1% SDS, 1× PBS, 50 mM N-ethylmaleimide from Sigma, and a protease inhibitor cocktail from Roche). After the centrifugation of lysates at 16,000 × *g* at 4 °C for 5 min, the supernatant was applied to a PD10 desalting column (GE Healthcare) previously equilibrated with binding buffer (3 M urea, 1 M NaCl, 0.25% SDS, 1× PBS and 50 mM N-ethylmaleimide). Eluates, except 50 μl kept as input fraction, were incubated with 250 μl of NeutrAvidin agarose beads (Thermo Scientific) for 40 min at room temperature and further 2 h and 20 min at 4 °C with gentle rolling. The material bound to the beads was washed with the following washing buffers (WB) (buffer composition can be found below): twice with WB1, thrice with WB2, once with WB3, thrice with WB4, once again with WB1, once with WB5, and thrice with WB6. The ubiquitylated material, still bound to the beads, was then eluted by heating the beads at 95 °C for 5 min in 125 μl of elution buffer (250 mM Tris-HCl, pH 7.5, 40% glycerol, 4% SDS, 0.2% bromophenol blue, and 100 mM DTT). Finally, samples were centrifuged at 16,000 × *g* at room temperature for 2 min in a Vivaclear Mini 0.8 μm PES-micro-centrifuge filter unit (Sartorious) to discard the NeutrAvidin resin. The composition of the washing buffers used for the biotin pulldown assays were: WB1, 8 M urea, 0.25 SDS, 1× PBS; WB2, 6 M guanidine-HCl, 1× PBS; WB3, 6.4 M urea, 1 M NaCl, 0.2% SDS, 1× PBS; WB4, 4 M urea, 1 M NaCl, 10% isopropanol, 10% ethanol, 0.2% SDS, 1× PBS; WB5, 8 M urea, 1% SDS, 1× PBS; WB6, 2% SDS, 1× PBS.

Before proceeding with mass spectrometry, inputs and eluted fractions were analyzed by immunoblotting with mouse anti-FLAG (1:1000, M2 clone, cat. no. F1804, Sigma-Aldrich), goat anti-Biotin-HRP (HRP, Horseradish Peroxidase-conjugated,1:1000) cat. no. 7075, Cell Signaling Technology, CST) and mouse anti-alpha-Tubulin (1:500, cat. no. AA4.3, DSHB) antibodies.

In-gel trypsin digestion and peptide extraction

Ubiquitylated material eluted from biotin pulldown assays was concentrated in a Vivaspin 500 centrifugal filter units (Sartorius) and resolved by SDS-PAGE in 4–12% Bolt Bis-Tris precast gels (Invitrogen). Proteins were visualized with GelCode blue stain reagent (Invitrogen) and gel lanes were cut into 4 slices to remove known endogenously biotinylated proteins and avidin monomers, as previously described[47]. Selected slices were subjected to in-gel trypsin digestion[48] with minor modifications. Proteins were reduced with DTT (10 mM in 50 mM NH4HCO3, 56 °C, 45 min), alkylated with chloroacetamide (25 mM in 50 mM NH4HCO3, room temperature, 30 min, dark) and incubated with trypsin (12.5 ng/ml in 50 mM NH4HCO3, 37 °C, overnight). The supernatant was recovered, and peptides were extracted twice from the gel: first, with 25 mM NH4HCO3 and acetonitrile and then with 0.1% trifluoracetic acid and acetonitrile. The recovered supernatants and the extracted peptides were pooled, dried in a SpeedVac (Thermo Fisher Scientific) and subsequently desalted with homemade C18 tips (3M Empore C18).

Liquid Chromatography with tandem Mass Spectrometry (LC-MS/MS)

An EASY-nLC 1200 liquid chromatography system interfaced with a Q Exactive HF-X mass spectrometer (Thermo Scientific) via a nanospray flex ion source was employed for the mass spectrometric analyses. Peptides were loaded onto an Acclaim Pep-Map100 pre-column (75 μm × 2 cm, Thermo Scientific) connected to an Acclaim PepMap RSLC C18 (75 μm × 25 cm, Thermo Scientific) analytical column. Peptides were eluted from the column using the following gradient: 18 min from 2.4 to 24%, 2 min from 24 to 32% and 12 min at 80% of acetonitrile in 0.1% formic acid at a flow rate of 300 nl min^{-1}. The mass spectrometer was operated in positive ion mode. Full MS scans were acquired from m/z 375–1800 with a resolution of 120,000 at m/z 200. The 10 most intense ions were fragmented by higher energy C-trap dissociation with normalized collision energy of 28. MS/MS spectra were recorded with a resolution of 15,000 at m/z 200. The maximum ion injection times were 100 ms and 120 ms, whereas AGC target values were 3 × 106 and 5 × 105 for survey and MS/MS scans, respectively. In order to avoid repeat sequencing of peptides, dynamic exclusion was applied for 12 s. Singly charged ions or ions with unassigned charge state were also excluded from MS/MS. Data were acquired using Xcalibur software (Thermo Scientific).

MS data processing and bioinformatics

Acquired raw data files were processed with the MaxQuant[49] software (version 1.6.0.16) using the internal search engine Andromeda[50] and tested against the UniProt database filtered for *Drosophila melanogaster* entries (release 2017_11; 43,868 entries). Mass tolerance was set to 8 and 20 ppm at the MS and MS/MS level, respectively. Enzyme specificity was set to trypsin, allowing for a maximum of three missed cleavages. Match between runs option was enabled with 1.5 min match time window and 20 min alignment window to match identification across samples. The minimum peptide length was set to seven amino acids. The false discovery rate for peptides and proteins was set to 1%. Normalized spectral protein LFQ (Label Free Quantitation) intensities were calculated using the MaxLFQ algorithm[51].

MaxQuant output data were analyzed with the Perseus module (version 1.5.6.0)[52] in order to determine the proteins significantly enriched in each of the genotypes. During the procedure, contaminants, reverse hits, as well as proteins with no intensity were removed, as well as those proteins only identified by site and/or with no unique peptides. Protein abundance was determined by LFQ intensity. Missing intensity values were replaced with values from a normal distribution (width 0.3 and down shift 1.8), meant to simulate expression below the detection limit[52]. Statistically significant changes in protein abundance were assessed by two-tailed Student's *t* test.

Immunoblots from ^{bio}Ub pulldowns

In order to confirm the results obtained by mass spectrometry, ^{bio}Ub pulldowns were carried out using flies bearing GMR-Gal4, UAS-(^{bio}Ub)$_6$-BirA; UAS-FLAG-HA-Fbxo42/UAS-Ataxin-2-HA. All Biotin pulldown steps were identical to those described above, with the modification of the elution step. The elution of biotinylated proteins from the beads was performed with 4× Laemmli buffer (250 mM Tris-HCl pH 6.8, 40% glycerol, 8% SDS, 0.02% bromophenol blue) without reducing agents. Afterwards, the eluted volume was divided into two: half of the volume was incubated with 100 mM of DTT and heated at 65 °C for 20 min. Input and eluted samples (in the presence/absence of DTT) were loaded onto 7.5% Mini-Protean® TGX™ (Tris-Glycine eXtended) Precast Protein Gels (Bio-Rad) and immunoblots were performed with rat anti-HA (1:1000, 7C9, Chromotek) antibody.

Cell culture, transfections and RNAi treatments

Drosophila S2 cells were cultured at 24 °C without CO_2 in Schneider's *Drosophila* medium (Biowest) supplemented with 10% heat inactivated Fetal Bovine Serum (FBS, Biowest), 100 U/ml of penicillin plus 100 μg/ml of streptomycin (Thermo Fisher Scientific). The complete medium was filtered with 0.2 μm PES filter (VWR). S2 cells were transfected with the indicated plasmids using Effectene transfection reagent (QIAGEN) according to the manufacturer's instructions.

RNA-mediated interference (RNAi) was performed as described in ref. 53. Primer pairs bearing a 5' end T7 RNA polymerase binding site were used to PCR amplify specific sequences of the genes to be inhibited. PCR products (with ~500–600 bp in length) were then purified with NucleoSpin® Gel and PCR Clean-up kit (Macherey-Nagel, MN) or with NZYGelpure kit (NZYtech) and used as templates for dsRNA synthesis with T7 RiboMAX™ Express Large Scale RNA Production System (Promega). After the DNase treatment, dsRNAs were purified and concentrated with RNA Clean & Concentrator™-5 kit (Zymo Research).

Ubiquitylation assays in S2 cells

For the ubiquitylation assay, 5.0×10^5 S2 cells/ well were seeded in 6-well plates and treated with 25–30 μg of Fbxo42 dsRNA for 8 days. S2 cells endogenously expressing Fbxo42, and cells treated with Fbxo42 dsRNA were transfected with 200 ng of each one of the following plasmids: pActin-Gal4, pUAST-Ataxin-2-GFP and pUAST-His-Myc-Ubiquitin. Empty pUAST was used instead of pUAST-His-Myc-Ubiquitin as ubiquitylation control. 3 days after transfection, cells were incubated with 50 μM of MG132 (Z-Leu-Leu-Leu-al, C2211, Merck) for 4 h, to inhibit proteasome activity, and resuspended in lysis buffer (50 mM Tris-HCl pH 7.5, 150 mM NaCl, 1 mM EDTA, 0.5% Triton X-100) supplemented with protease inhibitors (cOmplete™, Mini, EDTA-free Protease Inhibitor Cocktail, Roche) and 0.7% of NEM. Cell extracts were harvested and incubated on ice for at least 30 min. To perform the pulldown of proteins conjugated with His-Ubiquitin, each cell lysate was incubated with 15 μl of a nickel-charged resin suspension (Profinity™ IMAC Ni-Charged Resin, cat. no. 156-0131, Bio-Rad) for 2 h and 20 min at 4 °C. Afterwards, resin was washed thrice in 1× PBS + 20 mM imidazole. The elution of the ubiquitylated molecules from the resin was performed with elution buffer containing 1× PBS + 250 mM imidazole at room temperature. The eluted volume was divided into two: half of the volume was incubated with 100 mM of DTT and heated at 65 °C for 20 min. Then, 4× Laemmli buffer (240 mM Tris-HCl pH 6.8, 8% SDS, 40% glycerol, 250 mM DTT, 0.04% bromophenol blue) was added to the samples (with/without DTT), and these were boiled for 5 min at 95 °C. Finally, samples were loaded onto 4–15% Mini-Protean TGX™ Precast Protein Gels (Bio-Rad) and immunoblots were performed with rat anti-GFP (1:1000, 3H9, Chromotek) and rat anti-Myc (1:2000, 9E1, Chromotek) antibodies.

In order to observe the effect of C244A mutation on Ataxin-2 ubiquitylation profile, the ubiquitylation assay was repeated, in this case, S2 cells were co-transfected with pActinGal4 and pUAST-Ataxin-2^{C244A}-GFP plasmids. All ubiquitylation assay steps were the same as those described above.

Co-immunoprecipitation

For co-immunoprecipitation of Fbxo42 and SkpA, S2 cells were transfected with pMT-SkpA-HA, pActinGal4, UAS-FLAG-HA-Fbxo42 or UAS-FLAG-HA-ΔFbxo42. Three days after, to induce the expression of SkpA-HA, 500 μM $CuSO_4$ was added to the culture media 24 h before harvesting the cells in lysis buffer (20 mM HEPES 7.5 pH, 5 mM KCl, 1 mM MgCl2, 0.1% NP-40) supplemented with protease inhibitors (cOmplete™, Mini, EDTA-free Protease Inhibitor Cocktail, Roche). The immunoprecipitation was done using Anti-FLAG M2 Affinity gel (A2220, Sigma).

For co-immunoprecipitation of Fbxo42 and Ataxin-2, S2 cells endogenously expressing Fbxo42 protein or treated with Fbxo42 dsRNA were transfected with pActinGal4 and pUAST-Ataxin-2-GFP plasmids. Three days after, cells were resuspended in lysis buffer (50 mM Tris-HCl pH 7.5, 150 mM NaCl, 1 mM EDTA, 0.5% Triton X-100) supplemented with protease inhibitors (cOmplete™, Mini, EDTA-free Protease Inhibitor Cocktail, Roche).

To produce fly head extracts for Co-IP of Fbxo42 and Ataxin-2, flies expressing: GMR-GAL4, UAS-(^{bio}Ub)$_6$-BirA/UAS-Ataxin-2-GFP; UAS-FLAG-HA-Fbxo42 or GMR-GAL4, UAS-(^{bio}Ub)$_6$-BirA/UAS-Ataxin-2-GFP; UAS-FLAG-Fbxl7 were used. Fly heads were collected and homogenized in lysis buffer (50 mM Tris-HCl pH 7.4, 150 mM NaCl, 1 mM EDTA, 1% Triton X-100) supplemented with protease inhibitors (cOmplete™, Mini, EDTA-free Protease Inhibitor Cocktail, Roche) using glass beads (0.5 mm Glass Beads, Scientific Industries) in a bead beater homogenizer.

Equal amounts of protein lysates were incubated with GFP-Trap agarose beads (ChromoTek GFP-Trap® Agarose) with rotation end-over-end for 2 hours and 30 minutes at 4 °C. After that, tubes were centrifuged at 2700 × *g* for 2 min at 4 °C. Then, GFP-Trap beads were washed three times in ice cold dilution buffer (10 mM Tris-HCl pH 7.5, 150 mM NaCl, 0.5 mM EDTA) supplemented with protease inhibitors (cOmplete™, Mini, EDTA-free Protease Inhibitor Cocktail, Roche). After the last wash, supernatants were removed and beads were resuspended in SDS-sample buffer (250 mM Tris-HCl pH 7.5, 40% glycerol, 4% SDS and 0.2% bromophenol blue). Finally, beads were boiled for 10 min at 95 °C to dissociate immunocomplexes from the GFP-Trap beads and eluted fractions were recovered after centrifugation for 2 min at room temperature. In the case of the fly samples, the elution volume was divided into two: to half of the volume was added 100 mM DTT and this was then heated at 65 °C for 15 min. Regarding the cell eluates, it was added 100 mM DTT to the entire eluted volume. Samples (inputs and eluates) were further analyzed by western blot with rat anti-GFP (1:1000, 3H9, Chromotek) and rabbit anti-Fbxo42 (1:1000) antibodies.

Cycloheximide chase experiments

Drosophila S2 cells were transfected with pActinGal4, wild-type or mutant versions of pUAST-Ataxin-2-GFP in the presence/absence of FLAG-HA-Fbxo42. Three days after transfection, cells were treated with 100 μg/ml cycloheximide (cat. no. J66901.03, Alfa Aesar) for 0, 6 and 12 h, to inhibit the protein translation. S2 cells treated with Fbxo42 RNAi or with control RNAi and transfected with pActinGal4 and pUAST-Ataxin-2-GFP were also incubated with cycloheximide as aforementioned. At the indicated timepoints, cells were resuspended in lysis buffer (50 mM Tris-HCl pH 7.5, 150 mM NaCl, 1 mM EDTA, 0.5% Triton X-100) supplemented with protease inhibitors (cOmplete™, Mini, EDTA-free Protease Inhibitor Cocktail, Roche). Total cell extracts were analyzed by immunoblotting with rat anti-GFP (1:1000, 3H9, Chromotek) and rabbit anti-Fbxo42 (1:1000) antibodies. Tubulin, detected with mouse anti-alpha-Tubulin antibody (1:500, AA4.3, DSHB) was used as loading control. Where indicated, 50 μM MG132 (Z-Leu-Leu-Leu-al, C2211, Merck) was added to the S2 cells to inhibit the proteosome.

Immunoblots

Fly extracts or cell lysates were prepared in the above-mentioned lysis buffers supplemented with protease inhibitors (cOmplete™, Mini, EDTA-free Protease Inhibitor Cocktail, Roche). Protein concentration was determined by *DC*™ Protein Assay Kit from Bio-Rad. Afterwards, samples were mixed with 4× SDS Laemmli buffer (240 mM Tris-HCl pH 6.8, 8% SDS, 40% glycerol, 250 mM DTT, 0.04% bromophenol blue) and boiled at 95 °C for 5 min. Proteins were size separated by SDS-PAGE and transferred onto nitrocellulose membranes of 0.2 μm

(Bio-Rad). Immunoblots were blocked with 5% non-fat milk in TBS-T containing 0.1% Tween-20 or in PBS-T containing 0.05-0.1% Tween-20 for 1 h. After blocking, membranes were incubated overnight at 4 °C with the following primary antibodies (Supplementary Table 2): mouse anti-alpha-Tubulin (1:500, AA4.3, DSHB), rabbit anti-Fbxo42 (1:1000), rat anti-GFP (1:1000, 3H9, Chromotek), rat anti-HA (1:1000, 7C9, Chromotek), mouse anti-HA (1:1000, 16B12 clone, BioLegend), rat anti-Myc (1:2000, 9E1, Chromotek), guinea-pig anti-Ataxin-2 (1:5000) (kind gift from Patrick Emery), goat anti-Biotin-HRP conjugated (1:1000, cat. no. 7075, CST) and mouse anti-FLAG (1:1000, M2 clone, cat. no. F1804, Sigma-Aldrich).

Membranes were washed 4× for 10 min in TBS-T or PBS-T and incubated with HRP-conjugated secondary antibodies respective to the primary antibodies' species, specifically, sheep anti-mouse HRP (1:10000, cat. no. NXA931, Cytiva), goat anti-rat HRP (1:2000, cat. no. R-05075-500, Advansta), goat anti-rabbit HRP (1:5000, product no. AS10 668, Agrisera) and goat anti-guinea pig HRP (1:5000, cat. no. PA128679, Thermo Scientific) for 2 h at room temperature. Membranes were washed 4× for 10 min in TBS-T/PBS-T, and the signal was developed using ECL™ Prime Western Blotting Detection Reagent (RPN2232, Cytiva) and detected using a Chemidoc XRS+ (Bio-Rad) or an iBright™ FL 1500 Imaging System (Thermo Fisher Scientific).

For Xbp1s-GFP immunoblot analysis, 3.0×10^6 cells were seeded in 25 cm^2 flasks and treated with 30 μg of Ataxin-2 dsRNA or LacZ dsRNA (control) for 10 days. S2 cells were then re-plated in 12-well plates (4.5×10^5 cells/well) and transfected with pUASTattb-Xbp1-HA-GFP$^{3'UTRspliced}$, pActinGal4 and empty pUAST plasmids. Three days after transfection, S2 cells were incubated with 5 mM DTT (to induce UPR activation) for 4 h and 8 h. Cell extracts were harvested at the indicated timepoints. Xbp1s-GFP protein levels were analyzed by immunoblot with rat anti-GFP (1:1000, 3H9, Chromotek) and tubulin was used as loading control, being detected with anti-alpha-Tubulin (1:500, AA4.3, DSHB). Ataxin-2 mRNA depletion was confirmed by RT-PCR before further analysis. The knockdown of Ataxin-2 protein was also analyzed by immunoblot with guinea pig anti-Ataxin-2 (1:5000).

iBright™ Analysis Software was used for densitometry. Statistical analysis was performed using GraphPad Prism 8 software. Two-way ANOVAs were performed as mentioned in the figure legends. p values refer to: $^{***}p < 0.001$, $^{**}p < 0.01$ and $^{*}p < 0.05$. Uncropped and unprocessed blots are provided in the Source Data file.

AlphaFold 3 structural predictions

We utilized AlphaFold 3 (https://alphafoldserver.com/) to predict the structure of the Ataxin-2/Fbxo42/Cullin-1/Skp-1/Rbx1/E2/Ub complex based on the protein sequences. Since AlphaFold struggles to accurately predict disordered or dynamic regions, we pre-processed the sequences by trimming large intrinsically disordered regions (IDRs), typically located in the N- and C-terminal tails. To identify these disordered regions, we employed the Metapredict V2[54,55] tool (https://metapredict.net/), which allowed us to remove these regions prior to structure prediction. This resulted in more stable poses with improved structural metrics. For the final AlphaFold 3 prediction, the sequences were: Ataxin-2 (aa 62–1084), Fbxo42 (aa 21–347 and 586–667), Cullin-1 (aa 11–774), Skp-1 (full length protein), Rbx1 (aa 47–122), E2 (effete, full-length protein) and Ub (full length protein). The resulting model was visualized using ChimeraX [56].

Sequential immunofluorescence and single molecule RNA fluorescence in situ hybridization (smFISH) in *Drosophila*

Single molecule RNA fluorescence in situ hybridization was performed with custom Stellaris RNA FISH probes labelled with Quasar 670 dye (LGC Biosearch Technologies) targeting the Xbp1 mRNA.

Sequential IF and smFISH was performed according to LGC Biosearch Technologies' recommendations. Briefly, larvae were dissected in 1× PBS and fixed in 4% PFA in 1× PBS for 1 h at room temperature. Tissues were then rinsed twice, 10 min each in 1× PBS followed by two washes in 0.1% Triton X-100. Subsequently, larval tissues were washed with 1× PBS and incubated with primary antibodies diluted in 1× PBS, overnight at 4 °C with gentle agitation. Primary antibodies used were the following: mouse anti-ELAV (1:200) (cat. no. 9F8A9, DSHB) and guinea-pig anti-Ataxin-2 (1:200).

After overnight incubation with primary antibodies, tissues were washed three times with 1× PBS and incubated with appropriate secondary antibodies (Jackson ImmunoResearch Laboratories) diluted in 1× PBS for 2 h at room temperature. Then, tissues were washed three times with 1× PBS, 10 min each, and incubated with freshly prepared Wash Buffer A, containing 1× Stellaris RNA FISH Wash Buffer A (cat. no. SMF-WA1-60, LGC Biosearch Technologies) and 10% (v/v) formamide (F9037, Sigma-Aldrich) in RNase free water, for 10 min at room temperature. Afterwards, samples were transferred to a 96-well plate and Wash Buffer A was discarded and replaced by freshly prepared Hybridization buffer [Stellaris RNA FISH Hybridization Buffer (cat. no. SMF-HB1-10, LGC Biosearch Technologies) + 10% (v/v) formamide] containing the Xbp1 probe set. Xbp1 probe stock (12.5 μM) was diluted 1:100 in Hybridization buffer to create a working probe solution of 125 nM. Larval tissues were incubated with Xbp1 probe solution in the dark at 37 °C, overnight.

The following day, Xbp1 probe solution was discarded, and unbound probes were removed by incubation with Wash Buffer A in the dark at 37 °C for 30 min. Tissues were mounted in VECTASHIELD® Antifade Mounting Medium with DAPI (Vector Laboratories, H-1200-10) and image acquisition was performed on a Zeiss LSM 880 confocal microscope.

Where indicated, the larval anterior parts' (containing the ring glands and eye imaginal discs) were exposed to 5 mM DTT for 4 h. Untreated tissues were used as control.

Single-molecule fluorescence in situ hybridization and immunofluorescence (smFISH-IF) in HeLa cells and data analysis

The combined smFISH-IF experiments in HeLa cells were conducted as previously described[57]. Briefly, HeLa 11ht cells in 1 mL culture medium [89% DMEM (Gibco), 10% (v/v) fetal bovine serum (Gibco) and 1% penicillin-streptomycin (Gibco)] were cultured in a 12-well plate (Greiner) at 37 °C with 5% CO_2. At 90% confluency, cells were either incubated with 1 μM thapsigargin-treated (TG, Alomone), 500 μM sodium arsenite (SA, Merck) or untreated culture medium for 2 h. Cells were then washed twice with PBS and fixed with 4% paraformaldehyde (Electron Microscopy Sciences) for 10 min at room temperature (RT), followed by permeabilization with PBS 0.2% Triton-X for another 10 min. Afterwards, a wash buffer [2× SSC (Invitrogen) and 30% v/v deionized formamide (Ambion)] containing 3% (w/v) BSA (Sigma) was used to pre-block cells for 30 min at RT. FISH probes targeting human XBP1 mRNA (Supplementary Table 3) were designed using the anglerFISH probe designer and were made by enzymatic oligonucleotide labeling using Atto565-NHS as described before[58]. Cells were first hybridized with hybridization buffer [150 nM smFISH probes, 2× SSC, 30% (v/v) formamide, 10% (w/v) dextran sulfate (Sigma)] for 4 h at 37 °C. Following three washes with wash buffer for 30 min, cells were incubated with primary antibody against human Ataxin-2 (1: 300, Proteintech, 1776-1-AP) at RT for 4 h. After two washes with PBS containing 0.1% (v/v) Tween-20 (Promega) for 30 min, the anti-rabbit IgG secondary antibody conjugated with ATTO 488 (1: 5000, Rockland, 611-152-122) was added for incubation of another 30 min. Coverslips were washed twice with PBS before mounting them onto microscopy slides using ProLong Gold antifade reagent incl. DAPI (Molecular Probes).

smFISH-IF images were acquired on a Nikon spinning disk microscope equipped with a Yokogawa CSU W1 scan head, a Plan-APOCHROMAT 100× 1.4 NA oil objective and iXon-888Life Back-illuminated EMCCD. Z-stacks were acquired with a step size of 0.2 μm. The

maximum laser intensities were employed for all the channels, with exposure times of 1000 ms for Atto565 (200 gain), 1000 ms for ATTO 488 (200 gain) and 200 ms for DAPI (400 gain), respectively.

Detection of single XBP1 mRNA spots in data from smFISH-IF experiments was performed in KNIME[59] analogous to what was previously described[60,61]. Briefly, individual Z-slices were projected as maximum intensity projections. Following background-substraction, XBP1 mRNA spots were detected using threshold-based spot detection. Nuclear segmentation was performed on the DAPI signal using the Huang thresholding method while cytoplasmic segmentation was done using the background signal in the immunofluorescence (Ataxin-2) channel and a manual intensity threshold. Final masks were generated via substraction of nuclear from cytoplasmic segmentations and the number of XBP1 mRNAs per cell was quantified as the number of spots in each of these masks. To quantify XBP1-Ataxin-2 colocalization, mean Ataxin-2 IF intensities in all pixel positions obtained from XBP1 spot detection were quantified and normalized to the average Ataxin-2 background intensity of each cell. Results were exported for subsequent statistical analysis in Excel and GraphPad Prism 10.

Individual nucleotide resolution UV cross-linking and immunoprecipitation (iCLIP)

The iCLIP method was carried out as described by Ule and collaborators[31,62] with some modifications according to the improved iCLIP (iiCLIP) method[32], namely i) the introduction of an infrared adapter as described in infrared-CLIP (irCLIP)[63], ii) using reverse transcriptase (RT) Superscript IV and RT primers that contain carbon spacers as in irCLIP, and iii) ampure beads-based purification of cDNAs. Briefly, S2 cells transfected with Ataxin-2-HA or Ataxin-2^{C244A}-HA were grown in 10 cm dishes. Three dishes were used per condition, including: a dish in which S2 cells were UV irradiated (+UV), a negative control in which no UV cross-linking was carried out (no UV) and an additional control in which UV irradiation was performed, although no antibody was used during the IP.

Three days after transfection, S2 cells of each condition were incubated with 5 mM DTT for 4 h (to induce UPR activation). After DTT incubation, the culture medium was removed, replaced by ice-cold PBS, and cells (from +UV and IgG dishes) were UV cross-linked twice with 0.15 J/cm^2 in a Stratalinker 2400 (Analytic Jena) at 254 nm. Next, cells were harvested by scraping and the cell suspensions were centrifuged at 500 × *g* at 4 °C for 5 min. Cell pellets were stored at −80 °C until use.

Cell pellets were lysed in iCLIP lysis buffer (50 mM Tris-HCl pH 7.4, 100 mM NaCl, 1% Igepal, 0.1% SDS, 0.5% sodium deoxycholate) supplemented with cOmplete protease inhibitor cocktail (Roche), and the protein concentration was determined using a BCA Protein Assay Kit (Thermo Scientific). To digest the genomic DNA and obtain RNA fragments of an optimal size range, each cell lysate was incubated with Turbo DNase (Invitrogen) and 0.4 U/ml of RNase I (Thermo Scientific) for exactly 3 min at 37 °C with shaking at 1100 rpm (in the thermomixer). After incubation on ice for 5 min, lysates were spun at 4 °C at 16,278 × *g* for 10 min, and supernatants were incubated with antibody-conjugated protein A/G Dynabeads (Thermofisher scientific) overnight at 4 °C. The antibodies were pre-conjugated to Protein A/G Dynabeads by incubating 100 µl of beads with 5 µg of either mouse Anti-HA (16B12 clone, BioLegend) or mouse IgG2b isotype control (MPC-11 clone, Tonbo Biosciences) for 1 h at room temperature. On the next day, supernatants were discarded, and beads were washed 3× with high-salt wash buffer (50 mM Tris-HCl pH 7.4, 1 M NaCl, 1 mM EDTA, 1% Igepal, 0.1% SDS, 0.5% sodium deoxycholate) and 1× with PNK wash buffer (20 mM Tris-HCl pH 7.4, 10 mM $MgCl_2$, 0.2% Tween-20). Beads were then transferred to a new tube and the 3′ end dephosphorylation was carried out: the magnetic beads were resuspended in a mixture containing T4 Polynucleotide Kinase (Thermo Scientific) and FastAP alkaline phosphatase (Thermo Scientific). Samples were incubated for 40 min at 37 °C with shaking at 1100 rpm; beads were washed once with 1× ligation buffer (50 mM Tris-HCl pH 7.5, 10 mM $MgCl_2$) and the on-bead ligation at room temperature (for 2 h) of the pre-adenylated adapter L7-IR to the 3′ ends of the RNAs was performed. Samples were then washed thrice with high-salt wash buffer and once with PNK wash buffer. To remove the excess of adapter, beads were resuspended in a removal mix containing 5′ deadenylase (NEB) and $RecJ_f$ exonuclease (NEB) and incubated for 30 min at 30 °C followed by 30 min at 37 °C whilst shaking at 1100 rpm. Beads were washed 3× with high-salt wash buffer and 1× with PNK wash buffer and the protein-RNA complexes were eluted in 1× NuPAGE loading buffer + 100 mM DTT at 70 °C for 1 min. The protein-RNA complexes were separated by SDS-PAGE in a 4–12% NuPAGE Bis-Tris gel (Invitrogen), transferred to a nitrocellulose membrane (Cytiva) for 2 h (at 30 V) and detected using infrared light on a Chemidoc MP (Bio-Rad).

The protein-RNA complexes were excised from the membrane using the infrared image printout as a mask, treated with a mix of proteinase K (Sigma-Aldrich) and PK + SDS buffer (10 mM Tris-HCl pH 7.4, 100 mM NaCl, 1 mM EDTA, 0.2% SDS) for 1 h at 50 °C whilst shaking at 1100 rpm. The membrane pieces were removed, samples were mixed with phenol: chloroform: isoamyl alcohol (Sigma-Aldrich), moved to a pre-spun 2 ml Phase Lock Gel Heavy tube and incubated for 5 min at 30 °C with shaking at 1100 rpm and phases were separated by centrifugation for 5 min at 16,278 × *g*. Next, chloroform (VWR) was added to the top phase, tubes were inverted to mix, and spun for 5 min at 16,278 × *g* at 4 °C. The aqueous layer was transferred into a new tube and the RNA was precipitated by adding 3 M sodium acetate pH 5.2 (Thermo Scientific), glycoblue (Invitrogen) and absolute ethanol, overnight at −20 °C. Samples were spun for 30 min at 21,130 × *g* at 4 °C, the supernatants were discarded, and RNA pellets were washed with 80% ethanol and resuspended in DEPC-treated water.

The RNAs were reversely transcribed into cDNAs using the Superscript IV (SSIV, Thermo Scientific), dNTP mix and barcoded RT primers (IDT) according to the manufacturer's instructions. Next, 1 M NaOH was added, and samples were incubated at 85 °C for 15 min for alkaline hydrolysis of the RNA. To neutralize the pH, the same amount of 1 M of HCl was added to the tubes. The cDNAs were purified using Mag-Bind Total Pure NGS beads (Omega Bio-Tek) following the manufacturer's instructions. The cDNAs were eluted in DEPC-treated water, circularized in a mixture containing CircLigase II ssDNA ligase with betaine additive (LGC Biosearch Technologies) for 2 h at 60 °C, and purified using the Mag-Bind Total Pure NGS beads.

The cDNAs were PCR amplified using an optimal number of cycles in a Phusion HF master mix (Thermo Scientific) containing P5/P7 Illumina sequencing primers. The amplified cDNA library was gel purified, the 150–400 bp fragments were incubated in crush-soak gel buffer (500 mM NaCl, 1 mM EDTA, 0.05% SDS) at 65 °C for 2 h 15 min, with 15 s of agitation at 1100 rpm and 45 s of rest, transferred to Costar SpinX columns (Corning), and spun at 16,278 × *g* for 5 min. The amplified cDNA was ethanol precipitated as described above, and resuspended in DEPC-treated water. Finally, the different (barcoded) cDNA libraries were mixed, purified using Mag-Bind Total Pure NGS beads, and sequenced at Genewiz (Azenta Life Sciences).

The iCLIP results were uploaded and analyzed on Flow bio (https://app.flow.bio) using the iCLIP pipeline as described https://docs.flow.bio/docs/clip-pipeline-1.0. In brief, 1) the demultiplexed reads were trimmed for the 3′end adapter sequence (AGATCGGAAGAGCACACGTCTGAA) by TrimGalore; 2) reads were pre-mapped to an index of non-coding RNA sequences using Bowtie; and the resulting unmapped reads mapped to the *Drosophila* genome (BDGP6.32 annotation) using STAR; 3) the aligned reads were deduplicated based on the unique molecular identifiers (UMI) and start position; 4) the crosslink positions were defined as the cDNA start position minus one in uniquely mapped reads; 5) positionally-enriched k-mer analysis[64] as performed to determine enriched motifs in high-scoring crosslinks,

using the following parameters: k-mer length as 5 nt (-k 5), proximal window as 20 nt (-w 20), distal window as 150 nt (-dw 150), and percentile parameter for assignment of 'thresholded' crosslinks to 0.7 (-p 0.7). All Ataxin-2 iCLIP data files generated, including the.bedgraph files of Fig. 5d, summary files of total crosslink counts in genes and RNA biotypes, and the parameters used in the iCLIP pipeline, are available on https://app.flow.bio/executions/5628194201944874 66. We selected the k-mers with highest PEKA scores and p value < 0.01 for Supplementary Fig. S5b. For the alignment of crosslinks at motif centers in the 3'UTR (Supplementary Fig. S5c), we normalized the crosslink counts at each meta position in the 3'UTR by the total number of crosslinks in the 3'UTR.

mRNA stability assay

For mRNA stability experiments, 3.0×10^6 cells were seeded in 25 cm^2 flasks and treated with 30 μg of Ataxin-2 dsRNA or LacZ dsRNA (control) for 10 days. S2 cells were then re-plated in 12-well plates (4.5×10^5cells/well) and transfected with pUASTattb-Xbp1-HA-GFP$^{3'UTRspliced}$[23], pActinGal4 and pUAST plasmids. Three days after transfection, S2 cells were incubated with 5 mM DTT (to induce UPR activation) for 4 h. Transcription was blocked with 5 μg/ml of actinomycin D (ActD, A9415, Sigma-Aldrich). Cells were incubated with ActD for 0, 1, 2 and 3 h and samples were collected at each indicated timepoint for RNA extraction using NZYtech Total RNA Isolation kit. RNA samples were treated with Turbo DNase (Thermo) to eliminate DNA contamination. Equal amounts of total RNA were retro-transcribed using RevertAid H Minus First Strand cDNA Synthesis Kit (Thermo/Fermentas). Each qPCR reaction was performed on 1/40 of the cDNA obtained, using SSoFast EvaGreen Supermix (Bio-Rad) according to the manufacturer's instructions and Bio-Rad CFX-96 as detection system. For each sample, the levels of mRNAs were normalized using rp49 as a loading control. Normalized data were then used to quantify the relative levels of mRNA using the $\Delta\Delta CT$ method.

Quantification and statistical analysis

The confocal images were analyzed using the Fiji software and the ZEN Imaging Software (Zeiss). The number of granules and their components were quantified manually. Statistical analysis was carried out using GraphPad Prism 8 software. Two-way ANOVAs were performed as mentioned in the figure legends. p values refer to: $^{****}p < 0.0001$, $^{***}p < 0.001$, $^{**}p < 0.01$ and $^{*}p < 0.05$.

Reporting summary

Further information on research design is available in the Nature Portfolio Reporting Summary linked to this article.

Data availability

The mass spectrometry results have been deposited to the ProteomeXchange Consortium with the dataset identifier PXD065621. The iCLIP results are available on https://app.flow.bio/executions/5628194201944874 66. Source data for each figure are provided with this paper as a source data file. The data supporting the findings of this study are also available from the corresponding author.

References

1. Walter, P. & Ron, D. The unfolded protein response: from stress pathway to homeostatic regulation. *Nat. Methods* **334**, 1081–1086 (2011).
2. Tabas, I. & Ron, D. Integrating the mechanisms of apoptosis induced by endoplasmic reticulum stress. *Nat. Cell Biol.* **13**, 184–190 (2011).
3. Rasheva, V. I. & Domingos, P. M. Cellular responses to endoplasmic reticulum stress and apoptosis. *Apoptosis* **14**, 996–1007 (2009).
4. Acostaalvear, D. et al. XBP1 controls diverse cell type- and condition-specific transcriptional regulatory networks. *Mol. Cell* **27**, 53–66 (2007).
5. Ryoo, H. D., Domingos, P. M., Kang, M.-J. & Steller, H. Unfolded protein response in a Drosophila model for retinal degeneration. *EMBO J.* **26**, 242–252 (2007).
6. Liao, T. S. V. et al. An efficient genetic screen in Drosophila to identify nuclear-encoded genes with mitochondrial function. *Genetics* **174**, 525–533 (2006).
7. Yoshida, H., Uemura, A. & Mori, K. pXBP1(U), a negative regulator of the unfolded protein response activator pXBP1(S), targets ATF6 but not ATF4 in proteasome-mediated degradation. *Cell Struct. Funct.* **34**, 1–10 (2009).
8. Golic, K. G. Site-specific recombination between homologous chromosomes in Drosophila. *Science* **252**, 958–961 (1991).
9. Arsham, A. M. & Neufeld, T. P. A genetic screen in Drosophila reveals novel cytoprotective functions of the autophagy-lysosome pathway. *PLOS ONE* **4**, e6068 (2009).
10. Liu, X. & Lengyel, J. A. Drosophila arc encodes a novel adherens junction-associated PDZ domain protein required for wing and eye development. *Dev. Biol.* **221**, 419–434 (2000).
11. Kang, M.-J. & Ryoo, H. D. Suppression of retinal degeneration in Drosophila by stimulation of ER-associated degradation. *Proc. Natl Acad. Sci.* **106**, 17043–17048 (2009).
12. Kang, M.-J., Chung, J. & Ryoo, H. D. CDK5 and MEKK1 mediate pro-apoptotic signalling following endoplasmic reticulum stress in an autosomal dominant retinitis pigmentosa model. *Nat. Cell Biol.* **14**, 409 (2012).
13. Dui, W., Lu, W., Ma, J. & Jiao, R. A systematic phenotypic screen of *F-box* genes through a tissue-specific RNAi-based approach in *Drosophila*. *J. Genet. Genom.***39**, 397–413 (2012).
14. Barbosa, P. et al. SCF-Fbxo42 promotes synaptonemal complex assembly by downregulating PP2A-B56. *J. Cell Biol.* **220**, e202009167 (2020).
15. Ramirez, J. et al. Proteomic analysis of the ubiquitin landscape in the Drosophila embryonic nervous system and the adult photoreceptor cells. *PLOS ONE* **10**, e0139083 (2015).
16. Bosch, J. A. et al. The Drosophila F-box protein Fbxl7 binds to the protocadherin Fat and regulates Dachs localization and Hippo signaling. *eLife* **3**, e03383 (2014).
17. Martinez, A. et al. Quantitative proteomic analysis of Parkin substrates in Drosophila neurons. *Mol. Neurodegener.* **12**, 29 (2017).
18. Ripin, N. & Parker, R. Formation, function, and pathology of RNP granules. *Cell* **186**, 4737–4756 (2023).
19. McClellan, A. J., Laugesen, S. H. & Ellgaard, L. Cellular functions and molecular mechanisms of non-lysine ubiquitination. *Open Biol.* **9**, 190147 (2019).
20. Kelsall, I. R. Non-lysine ubiquitylation: doing things differently. *Front. Mol. Biosci.* **9**, 1008175 (2022).
21. Dikic, I. & Schulman, B. A. An expanded lexicon for the ubiquitin code. *Nat. Rev. Mol. Cell Biol.* **24**, 273–287 (2023).
22. Mirth, C., Truman, J. W. & Riddiford, L. M. The role of the prothoracic gland in determining critical weight for metamorphosis in Drosophila melanogaster. *Curr. Biol. CB* **15**, 1796–1807 (2005).
23. Cairrão, F. et al. Pumilio protects Xbp1 mRNA from regulated Ire1-dependent decay. *Nat. Commun.* **13**, 1587 (2022).
24. Buddika, K., Ariyapala, I. S., Hazuga, M. A., Riffert, D. & Sokol, N. S. Canonical nucleators are dispensable for stress granule assembly in Drosophila intestinal progenitors. *J. Cell Sci.* **133**, jcs243451 (2020).
25. Ciechanover, A. & Schwartz, A. L. The ubiquitin-proteasome pathway: the complexity and myriad functions of proteins death. *Proc. Natl Acad. Sci. USA.* **95**, 2727–2730 (1998).
26. Abramson, J. et al. Accurate structure prediction of biomolecular interactions with AlphaFold 3. *Nature* **630**, 493–500 (2024).
27. Hundley, F. V. et al. A comprehensive phenotypic CRISPR-Cas9 screen of the ubiquitin pathway uncovers roles of ubiquitin ligases in mitosis. *Mol. Cell* **81**, 1319–1336.e9 (2021).

28. Yoshida, H., Matsui, T., Yamamoto, A., Okada, T. & Mori, K. XBP1 mRNA is induced by ATF6 and spliced by IRE1 in response to ER stress to produce a highly active transcription factor. *CELL* **107**, 881–891 (2001).
29. Coelho, D. S. et al. Xbp1-independent Ire1 signaling is required for photoreceptor differentiation and rhabdomere morphogenesis in Drosophila. *Cell Rep.* **5**, 801 (2013).
30. Coelho, D. S., Gaspar, C. J. & Domingos, P. M. Ire1 mediated mRNA splicing in a C-terminus deletion mutant of Drosophila Xbp1. *PLOS ONE* **9**, e105588 (2014).
31. König, J. et al. iCLIP reveals the function of hnRNP particles in splicing at individual nucleotide resolution. *Nat. Struct. Mol. Biol.* **17**, 909–915 (2010).
32. Lee, F. C. Y. et al. An improved iCLIP protocol. Preprint at https://doi.org/10.1101/2021.08.27.457890 (2021).
33. Yokoshi, M. et al. Direct binding of Ataxin-2 to distinct elements in 3′ UTRs promotes mRNA stability and protein expression. *Mol. Cell* **55**, 186–198 (2014).
34. Singh, A. et al. Antagonistic roles for Ataxin-2 structured and disordered domains in RNP condensation. *eLife* **10**, e60326 (2021).
35. Bakthavachalu, B. et al. RNP-granule assembly via Ataxin-2 disordered domains is required for long-term memory and neurodegeneration. *Neuron* **98**, 754–766.e4 (2018).
36. Majumder, M. et al. A novel feedback loop regulates the response to endoplasmic reticulum stress via the cooperation of cytoplasmic splicing and mRNA translation. *Mol. Cell. Biol.* **32**, 992–1003 (2012).
37. Alzahrani, M. R. et al. Newly synthesized mRNA escapes translational repression during the acute phase of the mammalian unfolded protein response. *PLOS ONE* **17**, e0271695 (2022).
38. Lu, M. et al. Opposing unfolded-protein-response signals converge on death receptor 5 to control apoptosis. *Nat. Methods* **345**, 98–101 (2014).
39. Pelizzari-Raymundo, D. et al. IRE1 RNase controls CD95-mediated cell death. *EMBO Rep.* **25**, 1792–1813 (2024).
40. Domingues, C. & Ryoo, H. D. Drosophila BRUCE inhibits apoptosis through non-lysine ubiquitination of the IAP-antagonist REAPER. *Cell Death Differ.* **19**, 470–477 (2012).
41. Huang, H.-W., Zeng, X., Rhim, T., Ron, D. & Ryoo, H. D. The requirement of IRE1 and XBP1 in resolving physiological stress during Drosophila development. *J. Cell Sci.* **130**, 3040–3049 (2017).
42. Grether, M. E., Abrams, J. M., Agapite, J., White, K. & Steller, H. The head involution defective gene of Drosophila melanogaster functions in programmed cell death. *Genes Dev.* **9**, 1694–1708 (1995).
43. Ryoo, H. D., Bergmann, A., Gonen, H., Ciechanover, A. & Steller, H. Regulation of Drosophila IAP1 degradation and apoptosis by reaper and ubcD1. *Nat. Cell Biol.* **4**, 432–438 (2002).
44. Xu, D., Li, Y., Arcaro, M., Lackey, M. & Bergmann, A. The CARD-carrying caspase Dronc is essential for most, but not all, developmental cell death in Drosophila. *Dev. Camb. Engl.* **132**, 2125–2134 (2005).
45. Zhang, Y., Ling, J., Yuan, C., Dubruille, R. & Emery, P. A role for Drosophila ATX2 in activation of PER translation and circadian behavior. *Science* **340**, 879–882 (2013).
46. Gareau, C. et al. Characterization of fragile X mental retardation protein recruitment and dynamics in Drosophila stress granules. *PLOS ONE* **8**, e55342 (2013).
47. Ramírez, J. et al. The ubiquitin ligase Ariadne-1 regulates neurotransmitter release via ubiquitination of NSF. *J. Biol. Chem.* **296**, 100408 (2021).
48. Shevchenko, A., Wilm, M., Vorm, O. & Mann, M. Mass spectrometric sequencing of proteins silver-stained polyacrylamide gels. *Anal. Chem.* **68**, 850–858 (1996).
49. Cox, J. & Mann, M. MaxQuant enables high peptide identification rates, individualized p.p.b.-range mass accuracies and proteome-wide protein quantification. *Nat. Biotechnol.* **26**, 1367–1372 (2008).
50. Cox, J. et al. Andromeda: a peptide search engine integrated into the MaxQuant environment. *J. Proteome Res.* **10**, 1794–1805 (2011).
51. Cox, J. et al. Accurate proteome-wide label-free quantification by delayed normalization and maximal peptide ratio extraction, termed MaxLFQ. *Mol. Cell. Proteom.* **13**, 2513–2526 (2014).
52. Tyanova, S. et al. The Perseus computational platform for comprehensive analysis of (prote)omics data. *Nat. Methods* **13**, 731–740 (2016).
53. Clemens, J. C. et al. Use of double-stranded RNA interference in Drosophila cell lines to dissect signal transduction pathways. *Proc. Natl Acad. Sci. USA* **97**, 6499–6503 (2000).
54. Emenecker, R. J., Griffith, D. & Holehouse, A. S. Metapredict: a fast, accurate, and easy-to-use predictor of consensus disorder and structure. *Biophys. J.* **120**, 4312–4319 (2021).
55. Emenecker, R. J., Griffith, D. & Holehouse, A. S. Metapredict V2: an update to metapredict, a fast, accurate, and easy-to-use predictor of consensus disorder and structure. Preprint at https://doi.org/10.1101/2022.06.06.494887 (2022).
56. Meng, E. C. et al. UCSF ChimeraX: tools for structure building and analysis. *Protein Sci.* **32**, e4792 (2023).
57. Gómez-Puerta, S. et al. Live imaging of the co-translational recruitment of XBP1 mRNA to the ER and its processing by diffuse, non-polarized IRE1α. *eLife* **11**, e75580 (2022).
58. Piskadlo, E., Eichenberger, B. T., Giorgetti, L. & Chao, J. A. Design, labeling, and application of probes for RNA smFISH. *Methods Mol. Biol. Clifton NJ* **2537**, 173–183 (2022).
59. Berthold, M. R. et al. KNIME - the Konstanz information miner: version 2.0 and beyond. *ACM SIGKDD Explor. Newsl.* **11**, 26–31 (2009).
60. Voigt, F., Eglinger, J. & Chao, J. A. Quantification of mRNA turnover in living cells: a pipeline for TREAT data analysis. *Methods Mol. Biol. Clifton NJ* **2038**, 75–88 (2019).
61. Voigt, F. et al. Detection and quantification of RNA decay intermediates using XRN1-resistant reporter transcripts. *Nat. Protoc.* **14**, 1603–1633 (2019).
62. Huppertz, I. et al. iCLIP: Protein–RNA interactions at nucleotide resolution. *Methods* **65**, 274–287 (2014).
63. Zarnegar, B. J. et al. irCLIP platform for efficient characterization of protein-RNA interactions. *Nat. Methods* **13**, 489–492 (2016).
64. Kuret, K., Amalietti, A. G., Jones, D. M., Capitanchik, C. & Ule, J. Positional motif analysis reveals the extent of specificity of protein-RNA interactions observed by CLIP. *Genome Biol.* **23**, 191 (2022).

Acknowledgements

We would like to thank Hyung Don Ryoo, Andreas Bergmann, Iswar Hariharan, Patrick Emery, the Bloomington Drosophila Stock Center, FlyORF and the Developmental Studies Hybridoma Bank (DSHB) for fly stocks, plasmids and antibodies. We would like to thank Hyung Don Ryoo, Avi Ashkenazi and Brenda Schulman for comments on the manuscript. We thank Julia Domingos (Insta: cenasdajul) for the art work in Fig. 7. The authors acknowledge Fundação para a Ciência e a Tecnologia, I.P. (FCT) for funding MOSTMICRO-ITQB (UIDB/04612/2020 and UIDP/04612/2020) and LS4FUTURE Associate Laboratory (LA/P/0087/2020). The project was funded by the grants LCF/PR/HR17/52150018 ('la Caixa' Foundation), FCT AGA-KHAN/541141368/2019 (FCT and Aga Khan Foundation), DL57/2016 to FC and SFRH/BD/130817/2017 to CS. Franka Voigt is supported by an SNF project grant (320030-228276). Ming Yang is supported by the China Scholarship Council (202306910003). UM, NO and JR are supported by MINECO grant PID2020-117333GB-I00 and by Eusko Jaurlaritza grant IT1473-22. The proteomic analysis was performed in the Proteomics Core Facility-SGIKER at the University of the Basque Country (UPV/EHU).

Author contributions

CCS designed the study, performed most experiments, analyzed data and wrote the manuscript. NS performed the genetic screen, identified

the Fbxo42 mutants and made Fbxo42 constructs. FC designed and performed the mRNA stability/qPCRs and Fbxo42/SkpA co-IP experiments. JR, NO and UM performed the ^{bio}Ub pulldowns and the mass spectrometry data analysis. CJG made Fbxo42 constructs. VIR performed the genetic screen. MLT performed S2 transfections and immunoblots for Fig. 6. CA supervised and analyzed data. ZH supervised and analyzed FISH data. MY and FV performed FISH in HeLa cells. TNC performed the AF3 prediction. PAG supervised and analyzed iCLIP data. PMD designed and supervised the study, performed the genetic screen, analyzed data and wrote the manuscript. All authors, except VIR (deceased 20/04/2023), read and edited the manuscript.

Competing interests

CJG is now an employee of Genentech, Inc., a member of the Roche Group. Other authors report no competing interests.

Additional information

Supplementary information The online version contains supplementary material available at https://doi.org/10.1038/s41467-025-62417-2.

Correspondence and requests for materials should be addressed to Pedro M. Domingos.

Peer review information *Nature Communications* thanks Mani Ramaswami and the other, anonymous, reviewer(s) for their contribution to the peer review of this work. [A peer review file is available.